Impaired vasopressin neuromodulation of the lateral septum leads to social behavior deficits in *Shank3B*^{+/-} male mice

Maria Helena Bortolozzo-Gleich[1], Guillaume Bouisset [1], Lan Geng[2,3], Antonia Ruiz Pino [1], Yuki Nomura [1], Shuting Han [4,5,6], Yulong Li [2,3] & Félix Leroy [1] ✉

The neuropeptide arginine-vasopressin (AVP) has been repeatedly associated with the autism spectrum disorder (ASD) but the underlying mechanisms remain unclear. As *Shank3B*^{+/-} male mice, a model of ASD, exhibit deficits in sociability and social aggression, we focused on the lateral septum (LS), a brain region involved in the regulation of motivated behaviors and observed reduced AVP inputs from the bed nucleus of the stria terminalis (BNST) to LS. Manipulating AVP release from the BNST to LS of wild-type male mice, we found that AVP promotes both sociability and social aggression. Blocking the vasopressin receptor 1a (AVPR1a) in LS impaired sociability, while blocking the receptor 1b (AVPR1b) disrupted social aggression. Consequently, selective activation of AVPR1a or AVPR1b rescued the respective behavioral deficits in *Shank3B*^{+/-} male mice. These findings reveal that AVP release in LS modulates two distinct social behaviors via different receptors and highlight a possible strategy to rescue sociability during ASD.

Impairment in social interactions is a hallmark of the autism spectrum disorder (ASD). Typical social deficits include initiating interactions, responding to the initiations of others, maintaining eye contact, sharing enjoyment, reading the non-verbal cues of others, and taking another person's perspective. Social interactions are tightly regulated by several neuropeptides, including arginine-vasopressin (AVP), and studies have linked changes in vasopressinergic neuromodulation to ASD[1-4]. Thus, variants in the adjacent AVP gene regions have been associated with ASD diagnosis and endophenotypes[3,5,6]. In addition, magnetic resonant imaging (MRI) revealed changes in structure and functional connectivity in brain regions containing AVP[7]. Moreover, AVP levels in the plasma of children with ASD or their mothers has been associated with autistic symptoms[8-12]. AVP can bind to four distinct receptors: AVP receptor 1a (AVPR1A), AVP receptor 1b (AVPR1B), AVP receptor 2 (AVPR2), and the oxytocin receptor (OXTR). Among these, AVPR1A, AVPR1B, and OXTR are primarily located in the central

nervous system and show a high degree of polymorphism in patients with autism spectrum disorder (ASD)[13-19]. In contrast, AVPR2 is predominantly expressed in the kidney[20].

In rodent, subcutaneous administration of AVP in male rats extended the duration of social memory[21]. Further investigations showed that ventricular injections of AVP in male rats immediately after initial encounters with stimulus animals enhanced social memory[22], similar to peripheral AVP administration. Stimulation of the supraoptic nucleus and paraventricular nucleus in male rats led to AVP release in the hypothalamus and facilitated social recognition[23], similar to direct infusion of AVP in LS[24,25]. Conversely, peripheral AVP antagonist injections impaired social recognition in intact male rats but had no effect on castrated ones[26], suggesting that sex hormones may indirectly influence social recognition through modulation of the AVP system. Central administration of anti-AVP serum also resulted in impaired social recognition in male rats[27]. Knocking out AVPR1a

[1]Instituto de Neurociencias CSIC-UMH, Avenida Santiago Ramon y Cajal, San Juan, de Alicante, Spain. [2]State Key Laboratory of Membrane Biology, Peking University School of Life Sciences, Beijing, China. [3]PKU-IDG/McGovern Institute for Brain Research, Beijing, China. [4]Brain Research Institute, University of Zurich, Zurich, Switzerland. [5]Neuroscience Center Zurich (ZNZ), University of Zurich, Zurich, Switzerland. [6]University Research Priority Program (URPP), Adaptive Brain Circuits in Development and Learning, University of Zurich, Zurich, Switzerland. ✉e-mail: felxfel@aol.com

impaired social recognition in male[28] but not in female[29] mice, although this effect was not seen in all AVPR1a-KO lines[30]. Knocking out AVPR1b also leads to a deficit in social recognition and social memory (including the Bruce effect) as well as decreased social aggression and social motivation[31]. Finally, intracerebral administration of AVP in male oxytocin receptor knockout mice lowers aggression and fully reverts social and learning defects by acting on AVPR1a receptors[32]. Despite the extensive evidence that AVP facilitates social interactions, the mechanisms by which defects in vasopressinergic neuromodulation may lead to the social interaction deficits exhibited by ASD patients and mouse models remain elusive.

The lateral septum (LS) is a key region of the limbic system that supports many social and affiliative behaviors, including sociability, social discrimination, and social aggression[33]. Autopsy and MRI studies of ASD patients have identified developmental changes in the septum[3,34,35]. In rodents, LS is richly innervated by vasopressinergic fibers and expresses AVP receptors[33]. Consequently, male Brattleboro rats lacking AVP showed impaired social recognition, which can be restored by micro-dialysis of AVP into LS[36]. While the source of septal AVP remained unclear for a long time[37,38], recent evidence suggests AVP inputs to LS in mice originate from the bed nucleus of the stria terminals (BNST) and promote social interactions[39]. In addition, our

previous results demonstrate that AVPR1b activation in LS facilitates social aggression in male mice[40].

Here, we hypothesize that impairment of AVP release from the BNST to LS leads to the social behavior deficits exhibited by Shank3B^{+/-} male mice, a mouse model of ASD[41]. We first show that sociability and intermale social aggression are decreased in Shank3B^{+/-} male mice. Then, we confirmed that AVP[+] fibers to LS originate from the BNST before investigating vasopressinergic modulation of LS in Shank3B^{+/-} mice. We found a decrease in AVP[+] fiber density in LS and AVP[+] cell bodies in BNST, as well as a decrease in Avpr1a mRNA expression in LS and BNST of mutant mice. This decrease correlated with fewer excitatory terminals impinging on BNST[AVP] neurons. Using calcium recording of BNST[AVP] neurons terminals in LS and a biosensor for AVP in male WT mice, we probed the function of septal AVP release and correlated the fibers activation and AVP release with sociability and social aggression. We then used chemogenetic, terminal-specific silencing and gene expression knockdown to demonstrate that release of AVP from BNST to LS promotes sociability and social aggression in male WT mice. Consistent with the lower density of BNST[AVP] neurons observed previously, AVP biosensor recordings in male Shank3B^{+/-} mice indicated a decrease in AVP release during sociability and aggression. We then infused AVP receptor-specific
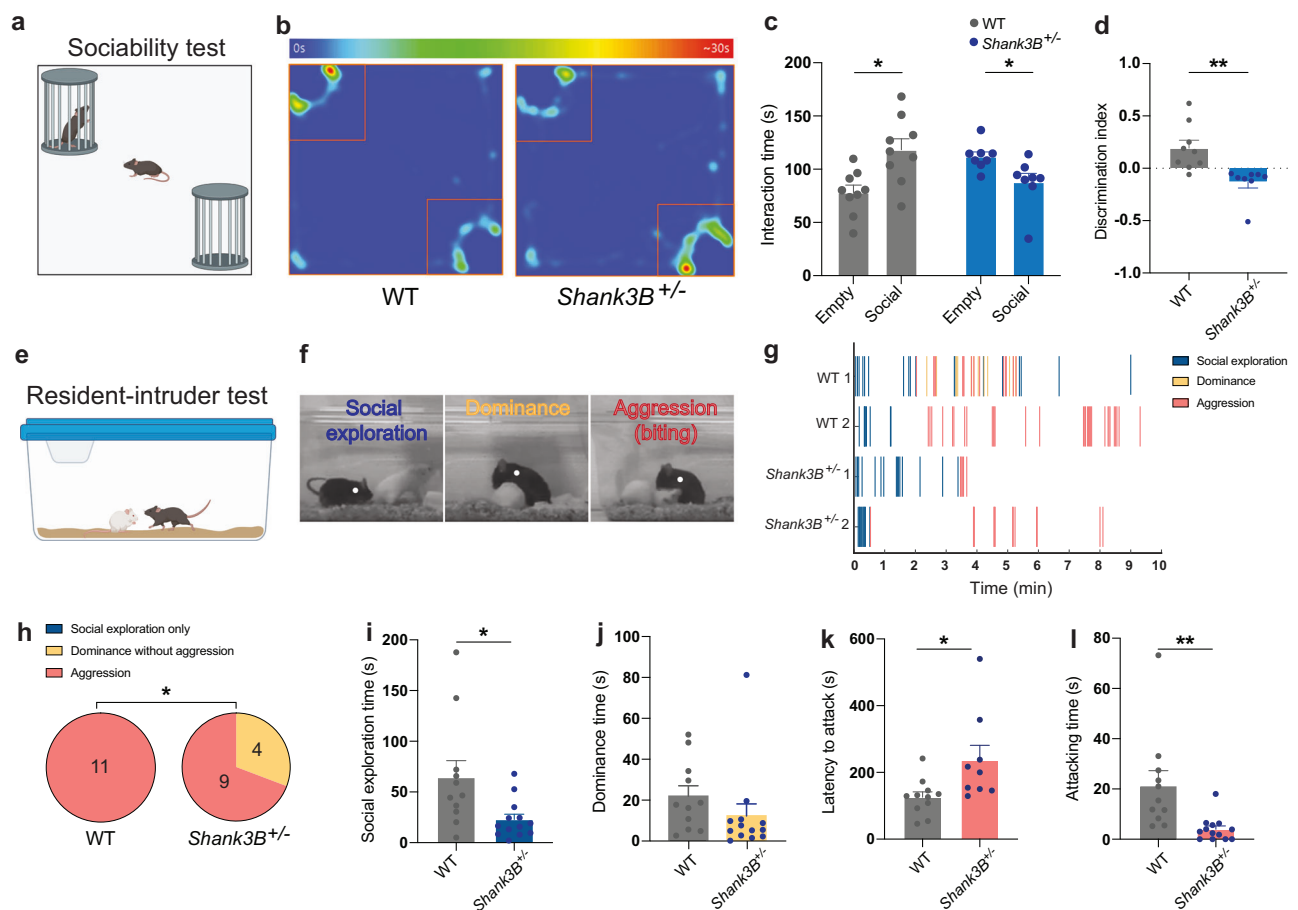

Fig. 1 | Sociability and social aggression are impaired in Shank3B^{+/-} mice.
a Schematic of the sociability test (Created in BioRender. Leroy, F. (2025) https://biorender.com/8v51vnv). **b** Heatmap of the accumulated time around the empty or social cup. **c** Time spent interacting with the empty or social cup (9/8 mice. Paired t test, WT: p = 0.03; Paired t test, Shank3B^{+/-}: p = 0.01). **d** Discrimination indexes for social preference (9/8 mice. Unpaired t test: p = 0.003). **e** Schematic of resident-intruder test (Created in BioRender. Leroy, F. (2025) https://BioRender.com/in0mntf). **f** Example frames showing social exploration, dominance, and aggression. **g** Raster plots showing social exploration, dominance, and aggression.

h Proportions of mice exhibiting only social exploration, social dominance without aggression or aggression (at least one biting attack) (11/13 mice. Chi-squared test: $\chi^2(1) = 4.06$, p = 0.04). **i** Social interaction duration (11/13 mice. Unpaired t test: p = 0.02). **j** Social dominance duration (11/13 mice. Unpaired t test: p = 0.2).
k Latencies to attack (11/9 mice. Unpaired t test: p = 0.02). **l** Attack durations (11/13 mice. Unpaired t test: p = 0.005). For the entire figure, bar graphs represent mean ± s.e.m. Each point is one mouse. * p < 0.05, ** p < 0.01, *** p < 0.001. Source data are provided as a Source Data file.
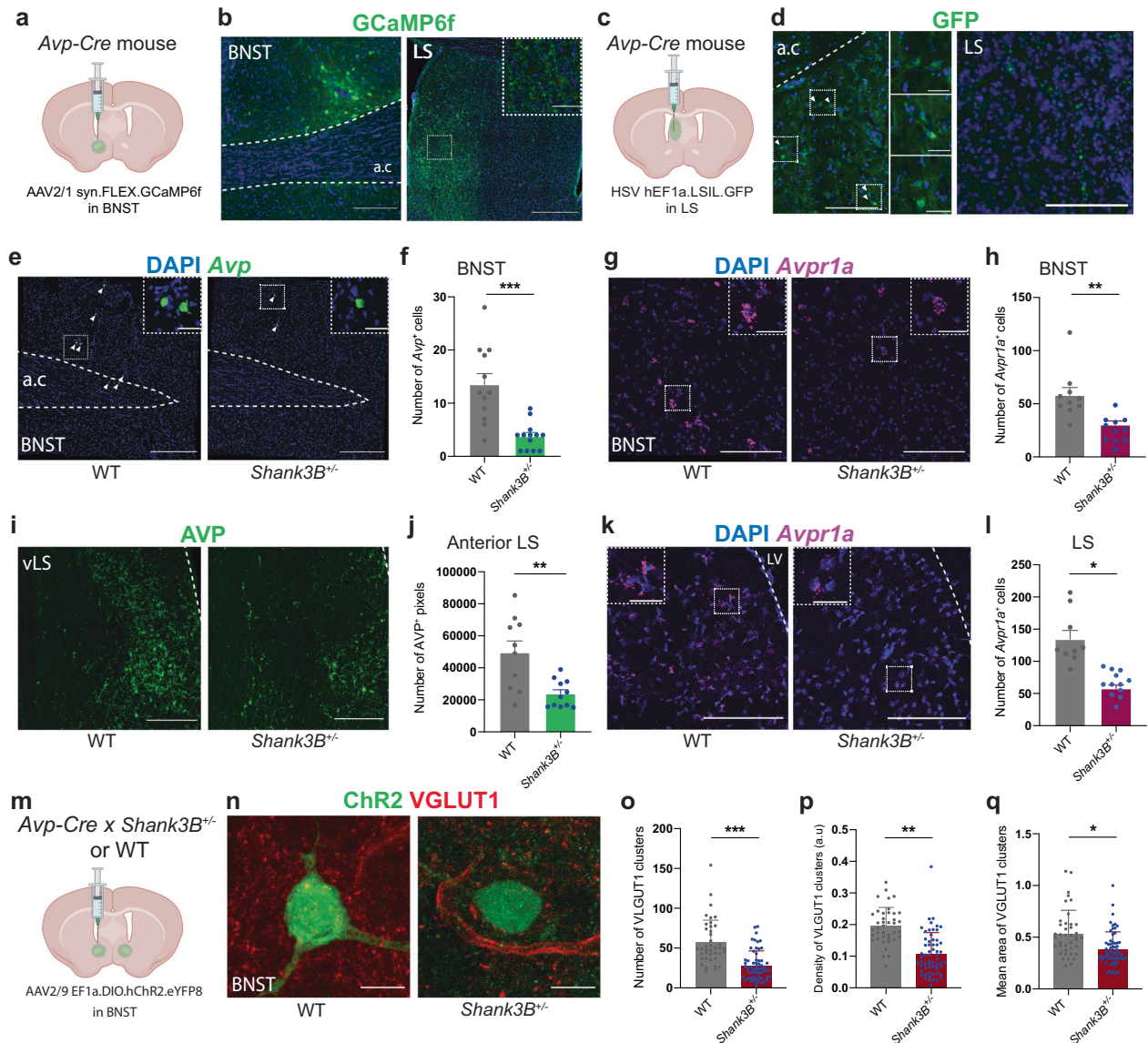
Fig. 2 | Vasopressinergic system from BNST (bed nucleus of stria terminalis) to LS (lateral septum) is decreased in *Shank3B*^{+/-} mice. a *Avp*-Cre mice injected unilaterally with AAV2/1 syn.FLEX.GcaMP6f.WPRE.SV40 in BNST (Created in BioRender. Leroy, F. (2025) https://BioRender.com/zzherf1). **b** Virally labeled AVP^{+} neurons in the BNST (left, scale: 400 μm) and AVP[+] fibers in LS (right, scale: 600 μm; zoom: 70 μm). **c** *Avp*-Cre mice injected in LS with hEF1a.LSIL.GFP (Created in BioRender. Leroy, F. (2025) https://BioRender.com/h1jqlsw). **d** Retrogradely labeled AVP^{+} neurons in BNST (scale: 200 μm; zoom: 50 μm) and AVP[+] fibers in LS (scale: 50 μm). **e, f** In situ hybridization picture of *Avp* mRNA in BNST (scale: 300 μm; zoom: 30 μm) and cell number (3 mice/group, 3 observations/mouse. Nested *t* test: *p* = 0.0001). **g, h** In situ hybridization picture of *Avpr1a* (scale: 200 μm; zoom: 50 μm) and cell number *in* WT and *Shank3B*^{+/-} mice (3 mice/group, 3 observations/mouse. Nested *t* test: *p* = 0.002). **i, j** Immunohistochemistry of AVP[+] fibers in anterior LS (scale: 400 μm) and quantification (10/11 mice/group. Unpaired *t* test: *p* = 0.002). **k, l** In situ hybridization for *Avpr1a* in LS (scale: 200 μm; zoom: 25 μm) and cell number (3 mice/group, 3 observations/mouse. Nested *t* test: *p* = 0.05). **m** *Avp*-Cre x *Shank3B*^{+/-} and WT mice injected in the BNST with AAV2/9EF1a.DIO.hChR2(E123T/T159C).eYFP (Created in BioRender. Leroy, F. (2025) https://BioRender.com/zzherf1). **n** BNST AVP^{+} cells labeled for YFP and VGLUT1 (scale: 10 μm). **o** VGLUT1 clusters per ROI (4/6 mice, 7 observations/mouse. Nested t test: *p* = 0.0003). **p** VGLUT1 clusters per ROI surface unit (4/6 mice, 7 observations/mouse. Nested t test: *p* = 0.003). **q** Mean area of VGLUT1 clusters (4/6 mice, 7 observations/mouse. Nested *t* test: *p* = 0.02). For the entire figure, bar graphs show mean ± s.e.m.; each point is one observation. *$p < 0.05$, **$p < 0.01$, ***$p < 0.001$. Source data are provided as a Source Data file.

antagonists in LS of WT mice and demonstrated that activation of AVPR1a in LS promotes sociability, while activation of AVPR1b is known to support social aggression[40]. Finally, we leveraged this functional segregation and activated one or the other septal AVP receptor in *Shank3B*^{+/-} mice in order to rescue sociability or social aggression.

Results

Sociability and social aggression are impaired in *Shank3B*^{+/-} mice

Prior studies have established that *Shank3B*^{+/-} mice exhibit both genetic and behavioral parallels to symptoms observed in autism spectrum disorder (ASD), where sociability/social investigation deficits are predominant[41,42]. However, the exploration of other potential social behavior deficits was never particularly investigated, prompting us to investigate whether *Shank3B*^{+/-} mice also exhibit changes in antagonistic behaviors, such as intermale social aggression. First, we confirmed the sociability deficits in *Shank3B*^{+/-} mice. Male *Shank3B*^{+/-} mice and WT littermates were introduced for 5 min in an open arena with two pencil cups in opposite corners. One pencil cup was empty while the other one had a C57Bl6/J mouse of the same age and sex (Fig. 1a). We measured the time the test mouse spent exploring each
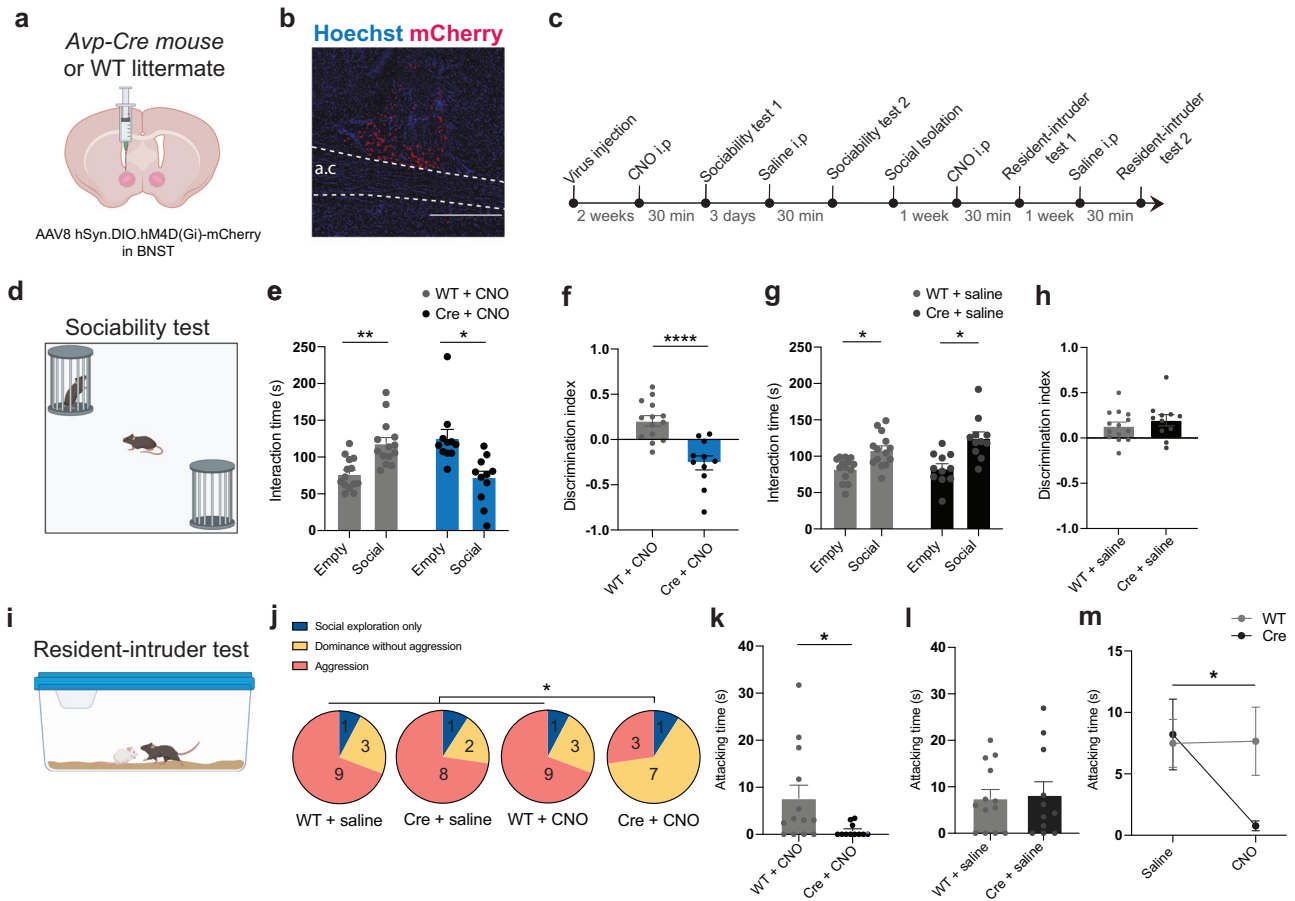
Fig. 3 | Silencing AVP+ neurons from the bed nucleus of the stria terminalis (BNST) impairs sociability and social aggression. a *Avp-Cre* mice and WT littermates injected bilaterally with AAV2/8 hSyn.DIO.hM4D(Gi)-mCherry in the BNST (bed nucleus of stria terminalis) (Created in BioRender. Leroy, F. (2025) https://BioRender.com/zzherf1). **b** Viral expression in the BNST of *Avp-Cre* mouse (scale bar: 300 µm). **c** Experimental timeline. **d** Schematic of the sociability test (Created in BioRender. Leroy, F. (2025) https://biorender.com/8v51vnv). **e** Interaction times with empty or social cup in CNO condition (14/11 mice. Paired t test WT + CNO group: *p* = 0.005; Paired *t* test Cre + CNO group: *p* = 0.02). **f** Discrimination indexes for social preference in CNO condition (14/11 mice. Unpaired *t* test: *p* < 0.0001). **g** Interaction times with social and empty cups in saline condition (14/11 mice. Paired *t* test, WT + saline: *p* = 0.01; Paired *t* test, Cre + saline: *p* = 0.01).

h Discrimination indexes for social preference in saline condition (14/11 mice. Unpaired *t* test: *p* = 0.4). **i** Schematic of the resident-intruder test (Created in BioRender. Leroy, F. (2025) https://BioRender.com/in0mntf). **j** Proportions of mice exhibiting only social exploration, social dominance without aggression, or aggression in CNO and saline conditions (13/11 mice. Chi-square test: χ²(2) = 7.39, *p* = 0.02). **k** Attack durations in CNO condition (13/11 mice. Unpaired *t* test: *p* = 0.03). **l** Attack durations in saline condition (13/11 mice. Unpaired *t* test: *p* = 0.83). **m** Attack durations between saline and CNO conditions (13/11 mice. Paired t test WT group: *p* = 0.91; Paired *t* test Cre: *p* = 0.02). For the entire figure, bar graphs represent mean ± s.e.m. Each point is one mouse. * *p* < 0.05, ** *p* < 0.01, *** *p* < 0.001, **** *p* < 0.0001. Source data are provided as a Source Data file.

pencil cup and found that while WT littermates exhibited a preference for the social cup, *Shank3B*^{+/-} male mice displayed sociability deficits (Fig. 1b–d) as previously reported[42].

Then, we tested the mutant mice for social aggression using the resident-intruder test, a behavioral assay designed to assess territorial intermale aggression[43]. Contrary to the sociability test, where the test mouse exhibits a preference but cannot fight, this test allows for direct interaction between two mice, where a wider range of social behaviors can be displayed (exploration, dominance, and aggression). Male *Shank3B*^{+/-} mice and WT littermates were single-housed for a week before a male Balb/cBy mouse of the same age was introduced into their home-cage. We chose to use Balb/cBy mouse intruders for their low aggressivity[44] in order to minimize the likelihood of attacks being initiated by the intruder (Fig. 1e). Typically, introducing an unfamiliar mouse into the home cage of a singly-housed resident prompted social exploration from the resident mouse, usually followed by social dominance behavior (see "Methods"). In some cases, social dominance eventually escalated to social aggression, defined as one or several biting bouts (Fig. 1f). These male-to-male interactions can be viewed as territorial interactions.

Shank3B^{+/-} mice showed a decrease in social exploration (similar to the result of the sociability test) and a tendency for a decrease in social dominance (Fig. 1l, j). Regarding the aggressive behavior, while all WT littermates escalated from social interaction to aggression within the 10 min duration of the test, only two-third of the *Shank3B*^{+/-} mice displayed social aggression (Fig. 1g–j). This difference led to an increase latency to attack and decreased attack duration (Fig. 1k, I). Overall, these results indicate that *Shank3B*^{+/-} mice display deficits in intermale social aggression in addition to sociability deficits.

To further analyze the differences in social exploratory behavior between WT littermates and mutant mice, we applied a supervised annotation method on movies acquired during a 2 min period in an open arena containing a male Balb/cBy mouse of the same age (Supplementary Fig. 1a). We measured the time mice spent in nose-to-nose and nose-to-tail interactions, as well as following a same-sex adult conspecific (Supplementary Fig. S1b, c). The results indicated no significant differences in nose-to-nose interactions, which can also be initiated by the stimulus mouse. However, they revealed a significant reduction in exploratory social behavior initiated by the test mouse in
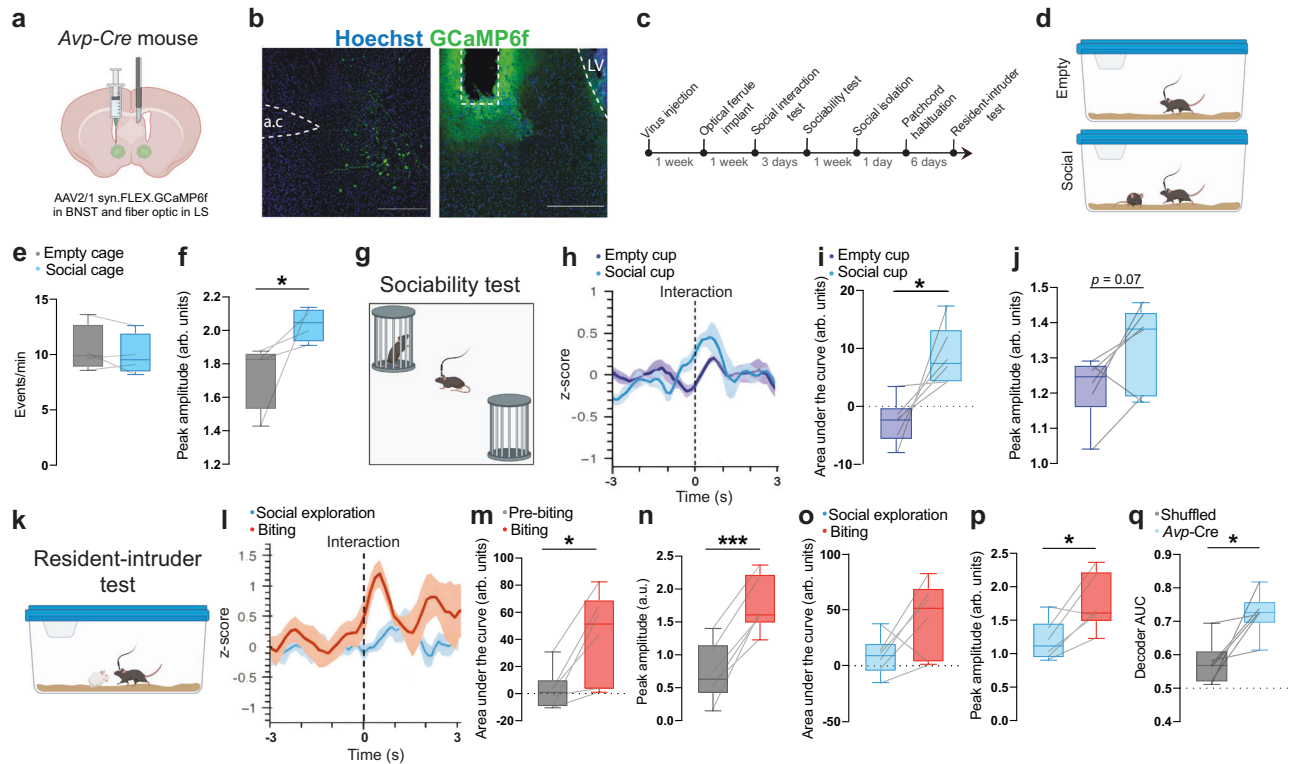
Fig. 4 | AVP⁺ axons from the bed nucleus of stria terminalis (BNST) to the lateral septum (LS) are activated during sociability and social aggression. a *Avp*-Cre mice injected bilaterally with AAV2/syn.FLEX.GcaMP6f.WPRE.SV40 in BNST with an optical ferrule in LS (created in BioRender. Leroy, F. (2025) https://BioRender.com/rj3w3d6). **b** Image of BNST and LS showing virally-labeled AVP⁺ cells (scale: 600 μm) and optical ferrule tip (scale bars: 400 μm). **c** Experimental timeline. **d** Schematic of the social interaction test (Created in BioRender. Leroy, F. (2025) https://BioRender.com/twqehea). **e** Frequencies of calcium transients before and during social interaction (4 mice. Paired *t* test: *p* = 0.4). **f** Amplitudes of the transients before and during social interaction (4 mice. Paired *t* test: *p* = 0.04). **g** Schematic of sociability test. **h** Peri-stimulus time histograms (PSTH) during interaction with each cup (6 mice) (Created in BioRender. Leroy, F. (2025) https://BioRender.com/yy20hso). **i** Areas under the curve of the PSTH during interaction with each cup (6 mice. Paired t test: *p* = 0.02). **j** Peak amplitudes of the PSTH during interaction with each cup (6 mice. Paired t test: *p* = 0.07). **k** Schematic of the resident-intruder test (Created in BioRender. Leroy, F. (2025) https://BioRender.com/vyq5lxl). **l** PSTH during social exploration and biting (6 mice). **m** Areas under the curve of the PSTH before and during biting (6 mice. Paired *t* test: *p* = 0.01). **n** Peak amplitudes of the PSTH before and during biting (6 mice. Paired *t* test: *p* = 0.0003). **o** Areas under the curve of the PSTH during social exploration and biting (6 mice. Paired *t* test: *p* = 0.08). **p** Peak amplitudes of the PSTH during social exploration and biting (6 mice. Paired *t* test: *p* = 0.02). **q** Performance of linear SVM decoders classifying social vs. non-social transients (6 mice. One-sided Wilcoxon signed-rank test: *p* = 0.02). For the entire figure, box plots show the median (central line) and the full range (minimum to maximum) across animals. PSTH plotted as mean ± s.e.m. Each point represents one mouse. * *p* < 0.05, ** *p* < 0.01, *** *p* < 0.001. Source data are provided as a Source Data file.

the mutant mice group (Supplementary Fig. 1d–f). There were no differences in the distance traveled during the test that could explain these findings (Supplementary Fig. 1g).

Vasopressinergic neuromodulation from the BNST to LS is dysregulated in *Shank3B*⁺/⁻ mice

We decided to investigate AVP inputs to the septum and injected the BNST of *Avp-Cre* mice with a Cre-dependent adeno-associated virus (AVV) expressing GCaMP6f (Fig. 2a). Three weeks later, we perfused the mice and observed GCaMP6f⁺ cells at the injection site and GCaMP6f⁺ fibers in LS (Fig. 2b). As the injection site was unilateral, we observed mostly ipsilateral projections. To confirm this BNST-LS AVP projection, we injected a Cre-dependent monosynaptic retrograde herpes simplex virus (HSV) expressing GFP in LS of *Avp-Cre* mice (Fig. 2c) and observed retrogradely labeled GFP⁺ cell bodies in posterior BNST as well as GFP⁺ axon fibers in LS (Fig. 2d). Since AVP is also expressed in the hypothalamus and central amygdala[38], we carefully looked for GFP⁺ cell bodies in these regions but could not find any. Overall, these results indicate that the BNST provides the major source of vasopressin to LS.

In order to investigate AVP release in LS in *Shank3B*⁺/⁻ mice, and since antibodies against AVP are known to poorly label AVP⁺ cell bodies

in the BNST[37,38], we relied on in situ hybridizations to label *Avp* and *Avpr1a* mRNAs in the BNST of *Shank3B*⁺/⁻ mice and WT littermates. We found a decrease in the number of *Avp*⁺ and *Avpr1a*⁺ cell bodies in the BNST of the mutant mice (Fig. 2e–h). Then, we used anti-AVP antibodies to label fibers and found a reduction in AVP⁺ pixels in anterior but not posterior LS (Fig. 2l, j and Supplementary Fig. 2a, b). Since AVP⁺ fibers in LS originate from the BNST, we can assume that the decrease in AVP⁺ in LS is due to a lower number of AVP⁺ cells in the BNST. Finally, we also observed a decrease in the number of *Avpr1a*⁺ cell bodies in LS (Fig. 2k, l). All together, these results indicate that the vasopressinergic neuromodulation from BNST to LS is impaired in *Shank3B*⁺/⁻ mice. Importantly, we did not find any difference in AVP⁺ cell number in the paraventricular nucleus of the hypothalamus, the region containing the highest density of AVP⁺ cells[38], suggesting that the dysregulation of AVP release is not generalized (Supplementary Fig. 2c, d).

SHANK proteins are multidomain scaffold proteins of the postsynaptic density of glutamatergic synapses and promote normal synaptic functioning[45]. As mutation of SHANK has been shown to lead to a decrease in excitatory synapses in the anterior cingulate cortex[46] and the hippocampal region CA1[47], we hypothesized that fewer glutamatergic synapses impinging onto BNST^AVP cells in *Shank3B*⁺/⁻ mice may lead to a decrease in their density. We injected the BNST of
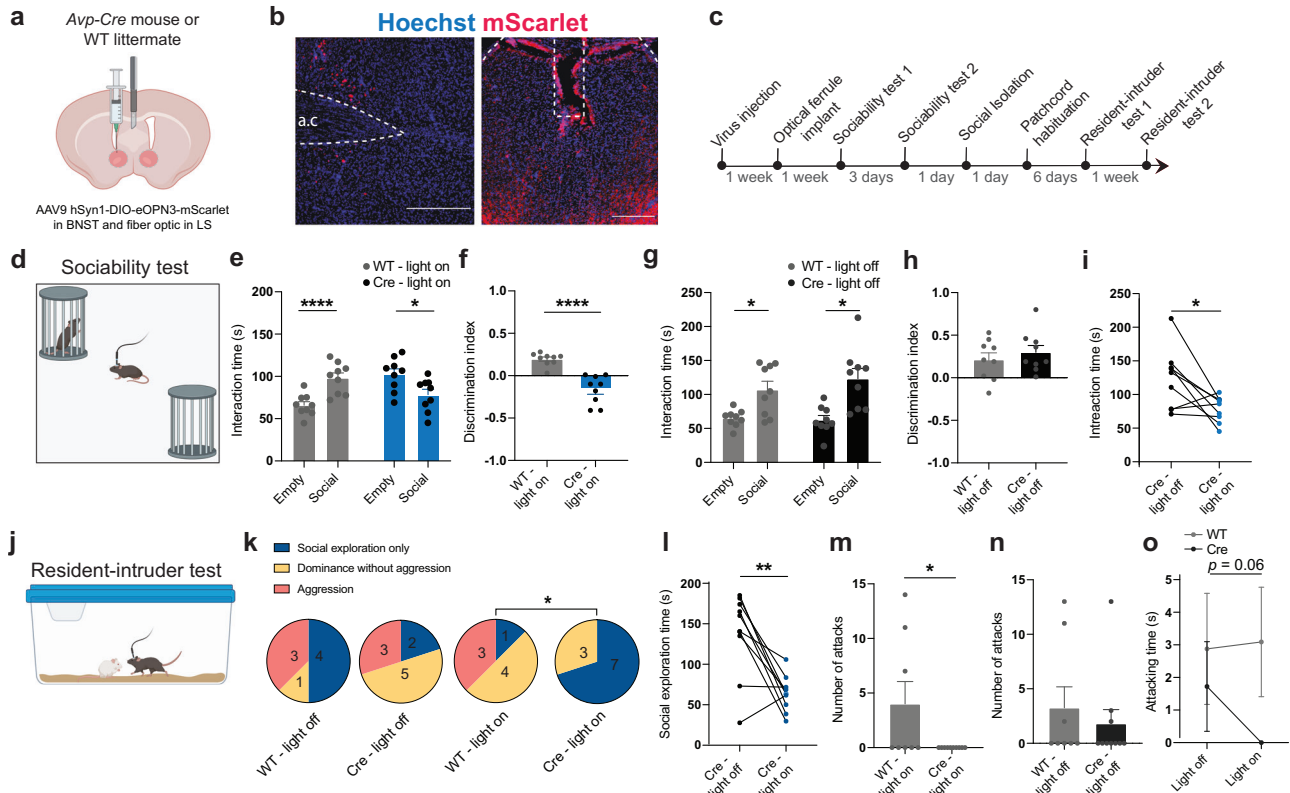
Fig. 5 | Silencing AVP⁺ terminals from the bed nucleus of the stria terminalis (BNST) to the lateral septum (LS) impairs sociability and social aggression.
a *Avp*-Cre mice and WT littermates injected bilaterally with AAV2/1hSyn1-DIO-eOPN3-mScarlet-WPRE in BNST with a fiber optic placed in LS (Created in BioRender. Leroy, F. (2025) https://BioRender.com/oa87ggm). **b** Images of BNST and LS showing AVP⁺ cells labeled with the virus (scale bar: 300 µm) and the trace of the optical ferrule tip (scale bar: 200 µm). **c** Experimental timeline. **d** Schematic of the sociability test (Created in BioRender. Leroy, F. (2025) https://BioRender.com/yy20hso). **e** Interaction times with empty and social cups in light-on condition (9 mice/group. Paired *t* test, WT: *p* < 0.0001; Cre: *p* = 0.02). **f** Discrimination indexes for social preference in light-on condition (9 mice/group. Unpaired t test: *p* < 0.0001). **g** Interaction times with social or empty cup in light-off condition (9 mice/group. Paired t test, WT: *p* = 0.02; Cre: *p* = 0.01). **h** Discrimination indexes for

social preference in the light-off condition (9 mice/group. Unpaired *t* test: *p* = 0.5). **i** Social interaction time in light-off vs. light-on condition for *Avp*-Cre mice (9 mice. Paired *t* test: *p* = 0.02). **j** Schematic of the resident-intruder test (Created in BioRender. Leroy, F. (2025) https://BioRender.com/vyq5lxl). **k** Proportions of mice showing only social exploration, social exploration and dominance without aggression, or aggression (8/10 mice. Chi-square test: χ²(2) = 7.51, *p* = 0.02). **l** Social exploration times in light-off and light-on conditions for *Avp*-Cre mice (9 mice. Paired *t* test: *p* = 0.002). **m** Number of attacks in light-on condition (8/10 mice. Paired *t* test: *p* = 0.04). **n** Number of attacks in light-off condition (8/10 mice. Unpaired *t* test: *p* = 0.5). **o** Attack durations between light-off and light-on (8/10 mice. Unpaired t test, light-off: *p* = 0.6; light-on: *p* = 0.06). For the entire figure, bar graphs show mean ± s.e.m. Each point is one mouse. * *p* < 0.05, ** *p* < 0.01, *** *p* < 0.001, **** *p* < 0.0001. Source data are provided as a Source Data file.

Avp-Cre x *Shank3B⁺/⁻* mice and WT controls with a Cre-dependent virus expressing channelrhodopsin coupled to YFP to label AVP⁺ cells in this region (Fig. 2m). After two weeks of viral expression, animals were perfused, and slices containing the BNST were labeled for the presynaptic vesicular glutamatergic transport VGLUT1 to quantify glutamatergic inputs (Fig. 2n).

We observed a strong reduction in the number, density, and size of VGLUT1⁺ clusters apposed to the BNST^AVP cells of *Shank3B⁺/⁻* mice (Fig. 2o–q), suggesting a reduced excitatory input for these cells. We made sure that although the ratio of VGLUT1⁺ pixels differed (Supplementary Fig. 3a), the mean area of the surface used to count VGLUT1⁺ clusters was unchanged (Supplementary Fig. S3). In addition, VLGUT1 cluster density in the entire BNST was not different between *Shank3B⁺/⁻* and WT littermates, indicating that the decrease in glutamatergic inputs is not global (Supplementary Fig. 3c, d).

To address whether the BSNT is involved in the social behavioral deficits observed in *Shank3B⁺/⁻* mice, we looked for differences in the expression of the immediate early gene c-fos following the resident-intruder test. We performed the resident-intruder test in *Shank3B⁺/⁻* mice and WT littermates. One hour later, we perfused the mice that displayed at least one aggressive episode and labeled the LS and BNST

for c-fos (Supplementary Fig. 4a, b). We found a decrease in c-fos⁺ cells in the posterior but not in the anterior BNST nor in anterior or posterior LS (Supplementary Fig. 4c–f). In addition, in situ hybridization showed that the posterior BNST contains a higher density of *Avp⁺* cells (22.9 ± 3.4 cells per mm²) compared to the anterior BNST (8.8 ± 1.0 cells per mm², Supplementary Fig. 5a, b).

Silencing BNST^AVP neurons impairs sociability and social aggression

What are the behavioral functions supported by BNST^AVP cells, and could a defect in AVP release from the BNST to LS induce the social behavioral deficits observed in *Shank3B⁺/⁻* mice? To address these questions, we used chemogenetic to silence BNST^AVP cells. *Avp-Cre* mice and WT littermates were injected in the BNST with a Cre-dependent AAV expressing an inhibitory DREADD tagged with mCherry. After 2 weeks, mice were injected intra-peritoneally with the DREADD agonist CNO 30 min prior to the sociability test (Fig. 3a–d). Unlike control littermates, *Avp-Cre* mice expressing iDREADD failed to prefer the social cup (Fig. 3e, f). A week later, we injected the same mice with saline and performed the same test. Here, both groups exhibited a preference for the social cup (Fig. 3g, h). Overall, silencing BNST^AVP cells impaired sociability/social exploration between male
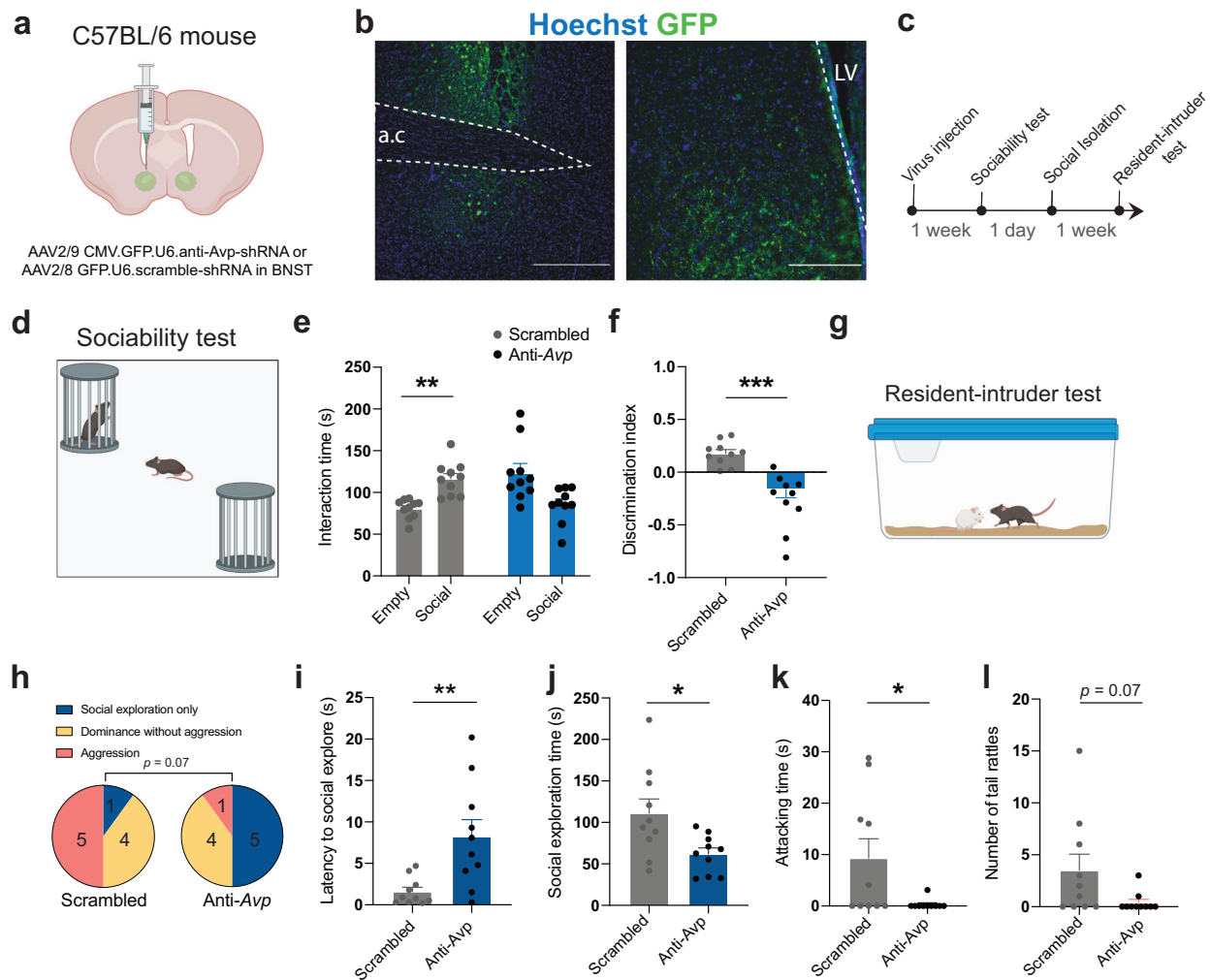
Fig. 6 | Knocking-down *Avp* expression in the bed nucleus of the stria terminalis (BNST) impairs sociability and social aggression. a WT mice bilaterally injected in the BNST with AAV2/9 CMV.GFP.U6.anti-*Avp*-shRNA or AAV2/8 GFP.U6.-scramble-shRNA (Created in BioRender. Leroy, F. (2025) https://BioRender.com/zzherf1). **b** Image of the BNST showing cells labeled with the virus (scale bar: 400 μm). Image of LS (lateral septum) with fibers anterogradely labeled with the virus (scale bar: 200 μm). **c** Experimental timeline. **d** Schematic of the sociability test (Created in BioRender. Leroy, F. (2025) https://biorender.com/8v51vnv). **e** Interaction times with empty and social cups (10 mice/group. Paired *t* test, scramble: $p = 0.001$; Paired *t* test, anti-*Avp*: $p = 0.06$). **f** Discrimination indexes for social preference (10

mice/group. Unpaired *t* test: $p = 0.0005$). **g** Schematic of the resident-intruder test (Created in BioRender. Leroy, F. (2025) https://BioRender.com/in0mntf). **h** Proportions of mice exhibiting only social exploration, social dominance without aggression, or aggression (at least one biting attack, 10 mice/group. Chi-squared test: $\chi^2(2) = 5.33$, $p = 0.07$). **i** Latencies to social explore during the resident-intruder test (10 mice/group. Unpaired *t* test: $p = 0.005$). **j** Social interaction duration (10 mice/group. Unpaired *t* test: $p = 0.02$). **k** Attack durations (10 mice/group. Unpaired *t* test: $p = 0.03$). **l** Number of tail rattles (10 mice/group. Unpaired *t* test: $p = 0.07$). For the entire figure, bar graphs represent mean ± s.e.m. Each point is one mouse. *$p < 0.05$, **$p < 0.01$ and ***$p < 0.001$. Source data are provided as a Source Data file.

mice. Mice were then singled housed for a week and subjected to the resident-intruder test following CNO injection (Fig. 3i). Only a small proportion of *Avp-Cre* mice demonstrated aggression as opposed to the majority of WT littermates (Fig. 3j). In addition, the time they spent attacking was decreased (Fig. 3k). A week later, the same mice were injected with saline and subjected to the same test. Both groups exhibited social aggression levels comparable to the WT littermates injected with CNO (Fig. 3l–m).

To better delineate the role of BNST^AVP cells, we also silenced these cells during additional tests on similar cohorts of mice. First, mice explored an open arena for 10 min in order to assess locomotor activity and anxiety (Supplementary Fig. 6a). *Avp-Cre* mice and WT littermates traveled the same distance and spent a similar amount of time in the center vs. surrounds (Supplementary Fig. 6b–d), suggesting that BNST^AVP cells do not regulate locomotion or anxiety. Then, we tested the mice for social novelty preference. Mice were introduced to an open arena containing 2 wire cups positioned

diagonally, each of which housed an unfamiliar, same-age mouse. Animals could freely explore for 5 min and were removed from the open arena and individually placed in a cage for 30 min. We then replaced one of the now familiar animals under the wire cup with an unfamiliar mouse. The test animals were reintroduced in the arena and had the possibility to socially interact freely for 5 min with the familiar or novel stimulus mouse (Supplementary Fig. 6e)[48]. Both groups exhibited social novelty preference, and total interaction times during learning or recall were similar (Supplementary Fig. 6e–i). Overall, BNST^AVP cells promote exploration and aggression of other males but do not support locomotion, anxiety, or social novelty preference.

BNST^AVP cell axonal projections to LS are activated during sociability and social aggression

We then used fiber photometry to image the AVP^+ terminals in LS. We bilaterally injected the BNST of *Avp-Cre* mice with a Cre-dependent
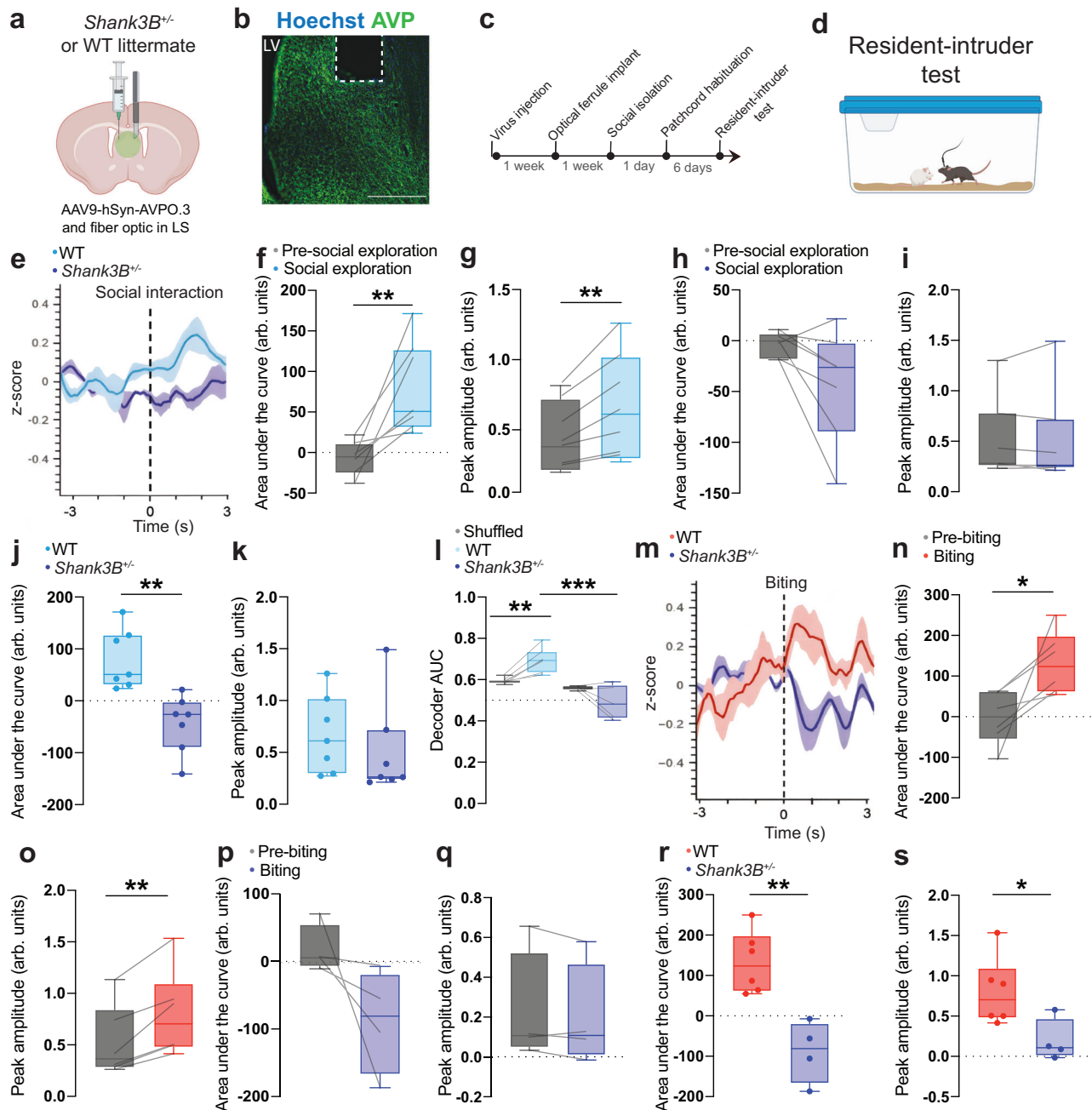
Fig. 7 | Septal AVP release is reduced in *Shank3B*+/- mice during social exploration and aggression. a WT and *Shank3B*+/- mice bilaterally injected with AAV9hSyn.AVP0.3 and implanted with an optical ferrule in the lateral septum (LS) (Created in BioRender. Leroy, F. (2025) https://BioRender.com/j3posib). **b** Image of trace of the optical ferrule tip in LS (scale bar: 400 µm). **c** Experimental timeline. **d** Schematic of the resident-intruder test (Created in BioRender. Leroy, F. (2025) https://BioRender.com/vyq5lxl). **e** Peri-stimulus time histogram (PSTH) during social exploration for WT and *Shank3B*+/- mice (7 mice/group). **f** Areas under the curve of the PSTH before and during social exploration for WT mice (7 mice. Paired *t* test: *p* = 0.009). **g** Peak amplitudes of the PSTH before and during social exploration for WT mice (7 mice. Paired *t*test: *p* = 0.006). **h** Areas under curve for *Shank3B*+/- mice (7 mice. Paired t test: *p* = 0.07). **i** Peak amplitudes for *Shank3B*+/- mice (7 mice. Paired *t* test: *p* = 0.9). **j** Areas under the curve during social exploration WT vs. *Shank3B*+/- mice (7 mice/group. Unpaired *t* test: *p* = 0.001). **k** Peak

amplitudes during social exploration for WT vs. *Shank3B*+/- mice (7 mice/group. Unpaired *t* test: *p* = 0.4). **l** Linear SVM decoder performance (7/5 mice. Wilcoxon signed-rank test WT: *p* = 0.01; *Shank3B*+/-: *p* = 0.91; WT vs. *Shank3B*+/-: *p* = 0.00). **m** PSTH during biting for WT vs. *Shank3B*+/- mice (6/4 mice/group). **n** Areas under cthe urve before and during biting for WT mice (6 mice. Paired *t* test: *p* = 0.03). **o** Peak amplitudes during pre-biting vs biting for WT mice (6 mice. Paired *t* test: *p* = 0.004). **p** Areas under curve for *Shank3B*+/- mice (4 mice. Paired *t* test: *p* = 0.14). **q** Peak amplitudes for *Shank3B*+/- mice (4 mice. Paired *t* test: *p* = 0.26). **r** Areas under cthe urve during biting for WT vs. *Shank3B*+/- mice (6/4 mice. Unpaired *t* test: *p* = 0.002). **s** Peak amplitudes during biting (6/4 mice. Unpaired *t* test: *p* = 0.04). For the entire figure, box plots show the median (central line) and the full range (minimum to maximum) across animals. Each point is one mouse. PSTH plotted as mean ± s.e.m. **p* < 0.05, ***p* < 0.01, ****p* < 0.001. Source data are provided as a Source Data file.

AAV expressing the calcium sensor GCaMP6f before implanting an optical ferrule above the LS. (Fig. 4a–c). Two weeks after viral injection, animals were subjected to a direct social interaction test, which consisted in 2 min of baseline recording in the home-cage followed by

2 min of presentation of a novel mouse (Fig. 4d). We calculated the frequency and amplitude of the GCaMP6f fluorescent signal during baseline and social presentation. No significant difference was observed in the frequency of the signal, but the amplitude of the signal

was higher in the social condition, indicating that BNST^AVP fibers to LS are activated during social encounters (Fig. 4e, f).

Three days after, we performed the sociability test while recording terminal activity (Fig. 4g). We calculated the peri-stimulus time histogram using the start of interaction either with the social or the empty cup to synchronize traces and found that the area under the curve of the calcium peak was larger when interacting with the social cup (Fig. 4h–i). Similarly, the peak amplitude showed a tendency to be larger when approaching the social cup (Fig. 4j). These results confirmed the previous results of the direct social interaction test.

After the sociability test, animals were isolated for a week before recording the calcium activity during the resident-intruder test (Fig. 4k). Here, we calculated the peri-stimulus time histogram using the start of interaction or biting to synchronize traces (Fig. 4l). First, we compared the peak amplitude and area under the curve during biting to 3 s baseline before the biting. Both measures were significantly higher during biting, indicating that the vasopressinergic fibers originating from the BNST in the LS are also active during an aggressive encounter (Fig. 4m, n). We then asked if there was a difference between the magnitude of AVP+ fiber responses to social interactions or social aggression. As mice usually explore the intruder during the initial phase of the resident-intruder test, we calculated the peri-stimulus time histogram aligned to the start of social interaction and compared both responses. Peak amplitude of the response was higher during biting than social interaction, but not the area under the curve (Fig. 4o, p). We then employed a linear support vector machine (SVM) decoder to classify social from non-social transients (see "Methods"). Decoder performance was compared to a shuffled baseline where transient labels were randomly permuted. The decoder performed better on actual recordings compared to the shuffled distribution, indicating that social and non-social transients contain distinct activity patterns (Fig. 4q). Overall, BNST^AVP fibers projecting to LS are active during social interactions and aggression, with social aggression recruiting the fibers more efficiently.

Silencing BNST^AVP cell projection to LS impairs sociability and social aggression

To prove that this vasopressinergic projection from BNST to LS is necessary to promote sociability and social aggression, we used an optogenetic silencing approach. We injected the BNST of *Avp-Cre* mice and WT littermates with a Cre-dependent AAV expressing an enhanced mosquito homolog of the vertebrate encephalopsin (eOPN3) that can suppress synaptic output through a brief illumination of the pre-synaptic terminals[49]. We then implanted an optical ferrule above LS (Fig. 5a, b). After 2 weeks of viral expression, we performed the sociability test twice. Each test was performed 3 days apart with the light on and off conditions counterbalanced for each mouse (Fig. 5c, d). With the light on, WT littermates displayed a preference for the social cup while *Avp-Cre* mice did not (Fig. 5e, f). Without light, however, both groups exhibited social preference (Fig. 5g, h). When comparing light conditions for the same mice, *Avp-Cre* mice displayed reduced interaction with the social cup when the terminals were inhibited (Fig. 5i). Animals were then single-housed for a week and habituated to the patch cord in their home-cage before performing the resident-intruder test with counterbalanced light conditions (Fig. 5c, j). In line with results from the sociability test, turning on the light decreased social exploration for A*vp-Cre* mice (Fig. 5k, l). We then analyzed the social aggression exhibited by each group. *Avp-Cre* mice displayed a decrease in the number of attack bout only when with the light on (Fig. 5m, n). Finally, when comparing the same mice across light conditions, *Avp-Cre* mice but not WT littermates displayed a tendency toward a decrease in total attack time (Fig. 5o). Overall, these results indicate that silencing BNST^AVP pre-synaptic terminals to LS impairs male to male sociability and intermale social aggression, therefore recapitulating the chemogenetic silencing of BNST^AVP cells

and demonstrating the importance of this projection in regulating these social behaviors.

Genetic silencing of *Avp* expression in the BNST impairs sociability and social aggression

We have demonstrated that BNST^AVP neurons projecting to LS promote sociability and social aggression, but it is unclear whether this is mediated by AVP release. To address this question, we used a short-hairpin RNA approach to silence *Avp* mRNA expression. We injected AAVs expressing a shRNA against *Avp* or a scrambled shRNA as well as GFP in the BNST of C57BL6/J WT mice and observed cell bodies labeled in the BNST and fibers in LS (Fig. 6a–c). Confirming the efficacy of our approach, AVP labeling in LS following anti-*Avp* shRNA expression in the BNST was decreased compared to control shRNA expression (Supplementary Fig. 7), similar to previous results[50]. After 1 week of viral expression (shRNAs under U6 promoter readily express within 1-2 days), mice performed the sociability test (Fig. 6d). While mice that expressed the scrambled shRNA demonstrated normal social preference, mice expressing the shRNA against *Avp* failed to prefer the social cup, suggesting that AVP release from BNST^AVP cells is necessary to support sociability (Fig. 6e, f). We subsequently single-housed animals for a week and subjected them to the resident-intruder test (Fig. 6g). In line with the results of the sociability test, mice expressing the shRNA against *Avp* exhibited a higher latency to interact and less interaction time during the resident-intruder test (Fig. 6h–j). Regarding aggressive behaviors, 5/10 control mice bit the intruder at least once during the test while only 1/10 mice expressing the shRNA against *Avp* did so (Fig. 6h). The attack duration was also decreased and there was a tendency for the number of tail rattles to decrease as well (Fig. 6k, l). Together, these results indicate that the release of AVP from BNST^AVP cells promotes social aggression in addition to sociability.

Septal AVP release is reduced in *Shank3B*^+/- mice during social exploration and aggression

Given the behavioral deficits exhibited by *Shank3B*^+/- mice and reduced density AVP+ fibers in their anterior LS, we sought to directly test whether septal AVP release during social interaction and social aggression was decreased in mutants compared to WTs. To achieve this, we leveraged a novel AVP biosensor called AVP0.3. *Shank3B*^+/- and WT littermate mice were injected with AAV9.hSyn.AVP0.3 into vLS (ventral lateral septum) to turn every neuron near the injection site into an AVP detector. Then, we implanted an optical ferrule above the injection site (Fig. 7a–c). After recovery, mice were subjected to the resident-intruder test while monitoring vasopressinergic events using fiber-photometry (Fig. 7d). Aligning the fluorescent signals from WT mice to the onset of social interactions revealed an increase in both the area under the curve and peak amplitude compared to baseline (Fig. 7f, g). Mutant mice, in contrast, failed to exhibit increased activity during social interactions (Fig. 7h, i). Then, we directly compared the area under the curve or peak amplitude between WT and *Shank3B*^+/- mice and observed that vasopressinergic events were significantly larger in WT mice (Fig. 7j, k). We then applied the same linear SVM decoder method as described previously to classify between social and non-social transients in WT and mutant mice. In WT, decoder performance on our recordings was significantly higher than the shuffled distribution, indicating distinct activity patterns between social and non-social transients, consistent with the calcium recordings results (Fig. 4q). In contrast, the decoder's performance was similar between the biosensor recordings from mutant mice and the shuffled distribution. Furthermore, decoder performance was lower in mutants compared to WT (Fig. 7l).

We also aligned the fluorescent signals to the biting onset and found that WT mice exhibited an increase in peak amplitude and a

higher area under the curve during biting compared to baseline (Fig. 7m−o). In contrast, no significant changes were observed in *Shank3B*^{+/-} mice (Fig. 7p, q). As for social exploration, direct comparisons of the area under the curve or peak amplitude during biting revealed that WT exhibited higher activity compared to mutants (Fig. 7r, s). Overall, these findings indicate that AVP release is reduced in *Shank3B*^{+/-} mice during social exploration or aggression of another male mouse.

Activation of AVPR1a and 1b rescues sociability and social aggression respectively in *Shank3B*^{+/-} mice

Since the release of AVP and subsequent activation of AVPR1a in LS are decreased in *Shank3B*^{+/-} mice, we sought to compensate for it by infusing receptor-specific agonizts in LS in order to rescue the social behavioral deficits exhibited by the mouse model of ASD. Prior studies have shown that septal AVPR1a and AVPR1b supports different social behaviors[51]. Indeed, knocking out AVPR1a impairs social discrimination, which can be rescued by in-trans expression of AVPR1a in LS[52]. On the other hand, AVPR1b is expressed at the presynaptic terminals of CA2 pyramidal neurons, where its activation facilitates the flow of information from CA2 to LS to promote social aggression[40]. In addition, infusion of the AVPR1b antagonist SSR149415 in dorsal LS abolishes social aggression[40]. First, to further characterize the effect of blocking AVPR1a or 1b on sociability, we implanted C57BL6/J WT mice with a cannula guide in LS and infused them with saline, SSR149415 (AVPR1b antagonist) or SR49059 (AVPR1a antagonist, Supplementary Fig. 8a, b). Each mouse was infused with one of the drugs in randomized order and subjected to 3 sessions of the sociability test (Supplementary Fig. 8c). Blocking of AVPR1a abolished sociability while blocking AVPR1b had no effect on it (Supplementary Fig. 8d, e). In addition, drug infusion had no effect on total interaction time with both cups and total distance traveled (Supplementary Fig. 8f, g). Overall, these results suggest a complete dichotomy of action of AVP in LS whereby activation of AVRP1a promotes sociability with no effect on social aggression, while activation of AVPR1b promotes social aggression with no effect on sociability. This is likely due to the organization of LS in parallel pathways, allowing separate regulation of different motivated behaviors[53].

Then, we implanted *Shank3B*^{+/-} mice with a cannula guide in LS and infused them with saline, the AVPR1b agonist DDAVP, or a combination of AVP and SSR149415 in order to activate AVPR1a while blocking AVPR1b since there is no valid AVPR1a agonist (Fig. 8a, b). First, each mouse was infused with one of the drugs in randomized order and subjected to 3 sessions of the sociability test (Fig. 8c). Activating AVPR1a in *Shank3B*^{+/-} mice rescued sociability, unlike activation of AVPR1b (Fig. 8d−f). In addition, drug infusion had no effect on total interaction time with both cups and total distance traveled (Supplementary Fig. 9a−c). Then, we isolated the mice for 1 week, and each mouse was infused with one of the drugs in randomized order and subjected to 3 sessions of the resident-intruder test (Fig. 8c, g). Here, activating AVPR1b in *Shank3B*^{+/-} mice increased social aggression unlike activation of AVPR1a as indicated by the number of mice showing attack (Fig. 8h) and the number of attack bouts (Fig. 8i). Activation of AVPR1b also induced a tendency toward an increase in tail rattling duration (Supplementary Fig. 9e), while activation of either receptor induced a tendency toward an increase in dominance behavior (Supplementary Fig. 9f). Overall, these results show that activation of AVRP1a in *Shank3B*^{+/-} mice rescues sociability with no effect on social aggression while activation of AVRP1b rescues social aggression with no effect on sociability.

Discussion

First, our results demonstrate the importance of AVP release in LS to facilitate social exploration between male mice and therefore promote sociability. The increase in social exploration led to an increase in

sociability when mice had the choice to explore an empty cup versus a cup containing another male mouse. Our results are similar to a recent study which utilized optogenetics to show that inhibiting BNST[AVP] cells reduces social investigation in male, but not in female mice, whereas stimulating the same cells increased social investigation in both sexes[39]. Further, they found that optogenetic stimulation of BNST[AVP] cell inputs to LS increased social investigation and some anxiety-like behavior in males but not in females[39]. Contrary to this study, we did not observe a change in anxiety when manipulating the activity of BNST[AVP] cells. This difference may stem from experimental reasons since we used the open arena test while they favored the elevated zero maze.

In addition to promoting social exploration, our results also demonstrate a function for AVP in promoting intermale social aggression. Indeed, male to male social exploration usually precedes social aggression, and both social interactions can be viewed as part of a continuum of territorial interaction behaviors facilitated by AVP release from the BSNT. Correlation between septal AVP release and social aggression was previously documented in male rats[54–56], but the source of AVP release in LS, as well as a direct causal link, remained missing. Despite a lack of evidence suggesting that vasopressin may originate from other sources that the BNST, we acknowledge that the AVP biosensor approach would respond to the release of AVP from any source, not just the BNST. In addition, we used virgin male mice with limited aggressive experience throughout this study since these two factors are known to increase aggression[57,58]. Overall, our findings are consistent with these and other studies involving the BNST in social aggression[59,60]. In addition, our previous study highlighted the role of presynaptic AVPR1b at the CA2 to LS synapse to facilitate social aggression without further investigating the source of AVP[40]. Now, we show that AVP is released from the BNST to LS to facilitate social aggression through AVPR1b-mediated potentiation of the CA2 to LS synapse. Interestingly, examination of the intruder-evoked immediate early gene activation in *Avpr1b*-KO male mice revealed a decrease in EGR-1 expression in the BNST, suggesting a lesser recruitment of the BNST in these mice during aggression[61]. This observation remained puzzling since AVPR1b is absent from the BNST[62]. Here, we propose that, because the BNST receives inputs from LS[63], hypo-activation of the BNST in *Avpr1b*-KO male mice likely stems from the decreased transmission of CA2 inputs to LS in the absence of pre-synaptic AVPR1b. A decrease in BNST activation may, in turn, decrease AVP release to LS. Disruption of this AVPR1b-dependent positive feedback loop between LS and the BNST would contribute to *Avpr1b*-KO male mice exhibiting less aggression[64]. In normal conditions, this loop might be responsible for the facilitation of aggression during repetitive intruder presentation[43], similar to the LS-ventral tegmental area loop involving dopamine release in LS[58,65].

In this study, we focused on male mice given the sexual dimorphism of the vasopressinergic projection from the BNST to LS[66,67] and the numerous factors regulating the differentiation of these cells. Thus, testosterone levels around P7 in rats determine the sexual differentiation of AVP projections to LS, and without testosterone, females and castrated males exhibit few BNST[AVP] inputs to LS[66]. Consequently, peripheral AVP antagonist injection impairs social recognition in intact male rats but has no effect on castrated ones[68]. The fact that females and castrated males are able to perform social discrimination suggests that other mechanisms can also support this behavior. In addition, AVP^{+} cells in the BNST and medial amygdala also express progesterone receptors, acting to suppress AVP expression in these regions[69]. As a result, progesterone injection in male rats impairs social recognition[70], which can be rescued by direct AVP infusion into LS[25]. Finally, ablation of the pineal gland[71] or depletion of norepinephrine from the olfactory bulb[72] also blocks AVP-mediated social recognition. Overall, these results suggest that AVP expression in the
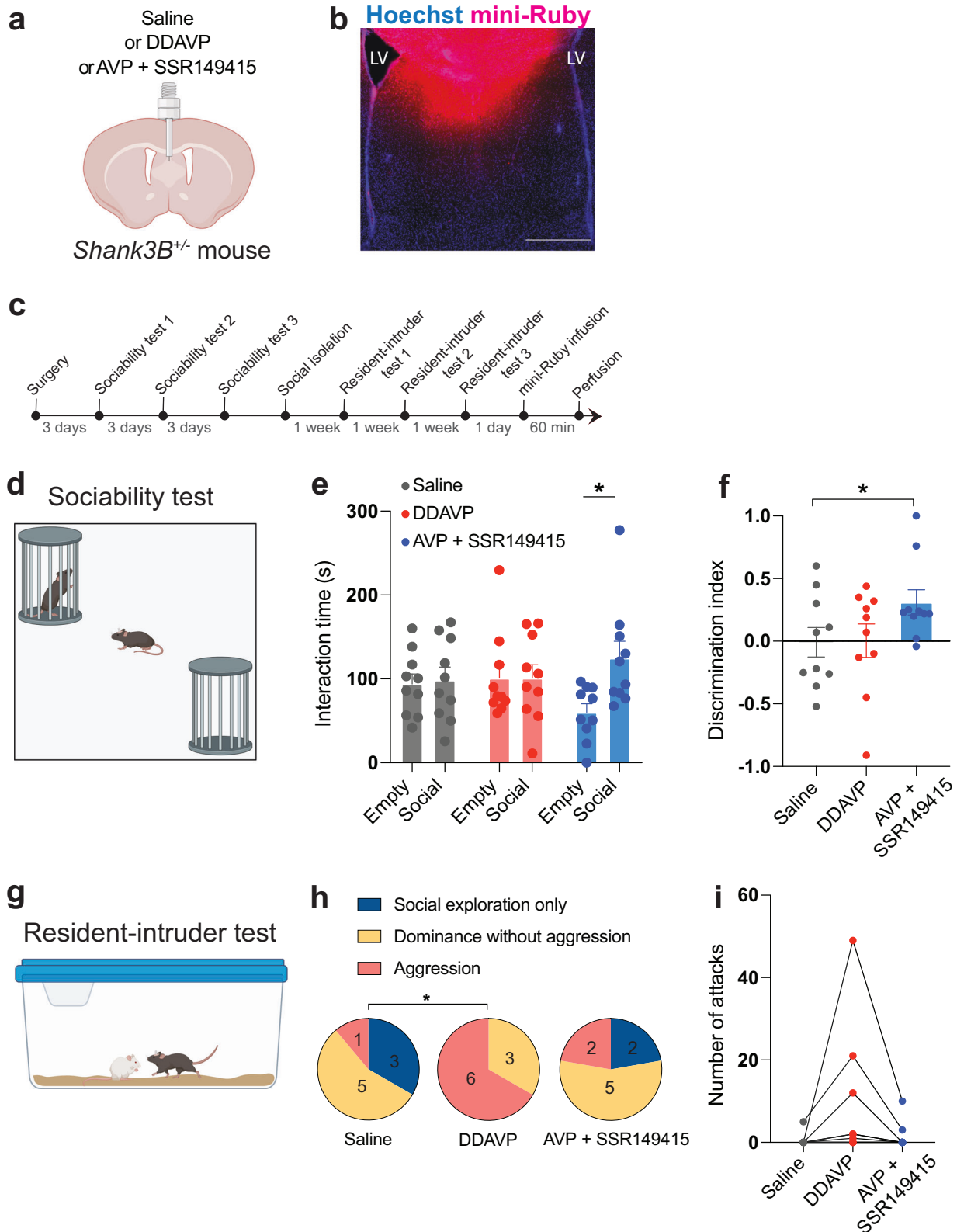
BNST is highly regulated in male rodents, particularly by reproductive hormones.

Female mice exhibit about half AVP$^+$ in BNST and less AVP$^+$ fibers in LS compared to males[67]. In addition, optogenetic inhibition in female mice did not affect social investigation, and optogenetic stimulation increased female investigation of males but not of females[39], suggesting that septal AVP release in female mice does not facilitate

social interactions to the same extent, confirming similar results in female rats[26,32]. Septal AVP release might even have an opposite role in female rodents since enhanced oxytocin release within the ventral LS, combined with reduced AVP release within the dorsal LS, is required for aggression in virgin female rats[73]. Similarly, blocking AVPR1a in LS increased social play behavior in males but decreased it in females[74,75], demonstrating opposite regulation of the same behavior in the same

Fig. 8 | Activation of AVPR1a or AVPR1b in LS of *Shank3B*^{+/-} mice rescues sociability or social aggression respectively. a *Shank3B*^{+/-} mice implanted in the dorsal middle of the septum with a guide cannula guide for drug delivery (Created in BioRender. Leroy, F. (2025) https://BioRender.com/ouq4aao). **b** Image showing the mini-Ruby localization in LS (scale bar: 600 μm). **c** Experimental timeline. After cannula guide implantation, *Shank3B*^{+/-} mice were infused with either saline, DDAVP, or AVP + SSR149415 before undergoing the sociability test. All animals were tested 3 times for sociability, with the infusion given in randomized order. Following social isolation, animals underwent 3 resident-intruder tests following the same infusions. **d** Schematic of the sociability test (Created in BioRender. Leroy, F. (2025) https://BioRender.com/irfm1dl). **e** Interaction times with empty and social cups (10 mice. Paired t test, saline condition: $p = 0.8$; Paired t test, DDAVP condition: $p = 1$; Paired t test, AVP + SSR149415 condition: $p = 0.04$). **f** Discrimination indexes

for social preference (10 mice). Repeated measures one-way ANOVA followed with Tukey's multiple comparisons test: $F = 4.35$, $p = 0.04$. Tukey's multiple comparisons test: Saline vs. DDAVP $p = 1$; Saline vs. AVP + SSR149415 $p = 0.02$; DDAVP vs. AVP + SSR149415 $p = 0.09$. **g** Schematic of the resident-intruder test (Created in BioRender. Leroy, F. (2025) https://BioRender.com/mjn7ex8). **h** Proportions of mice exhibiting only social exploration, social dominance without aggression or aggression (9 mice. Chi-squared tests: Saline vs. DDAVP $\chi^2(2) = 7.07$, $p = 0.03$; Saline vs. AVP + SSR149415 $\chi^2(2) = 0.53$, $p = 0.8$; DDAVP vs. AVP + SSR149415 $\chi^2(2) = 4.5$, $p = 0.1$). **i** Number of attacks (9 mice. Repeated measures one-way ANOVA: F (2, 8) = 3.07, $p = 0.1$). For the entire figure, bar graphs represent mean ± s.e.m. Each point is one mouse. *$p < 0.05$, **$p < 0.01$ and ***$p < 0.001$. Source data are provided as a Source Data file.

---

study. Further studies on the mechanisms of AVP release in female rodents are warranted to fully understand its function. Finally, AVPR1a antagonist infusion in the amygdala of rats impair impairs maternal memory but not the memory of other adults[76], which suggests that AVP release in different regions supports distinct types of social memory/preferences. Overall, whether AVP expression in the BNST of female rodents is subject to the same control remains to be explored.

Extending our findings to a pathological context, our results in *Shank3B*^{+/-} mice point to an impairment of AVP neuromodulation in LS due to a decrease in *Avp*^{+} cells in the BNST and *Avpr1a*^{+} cells in LS. This correlates with a decrease of VGLUT1^{+} excitatory terminals impinging on BNST[AVP] neurons. As SHANK3b is a presynaptic protein located on excitatory terminals, we propose that the mutation carried by the mutant mice led to a decrease in excitatory inputs received by BNST[AVP] neurons and consequently to their death. Interestingly, the decrease was specific to BNST[AVP] neurons and not general to the entire BNST, suggesting that the SHANK3b mutation does not affect every excitatory terminal to the same extent. We also found a decrease in *Avpr1a*^{+} cells in the BNST of the mutant mice. Given the 50 % overlap between *Avp*[+] and *Avpr1a*^{+} cells in the BNST (Supplementary Fig. 10a, b), we suppose that autocrine activation of these cells provides a negative feedback loop for AVP release. This may explain the negative correlation between AVP release and social aggression observed in the BNST[56]. AVP release from PVN to BNST might also dampen BNST[AVP] cell activity[77]. A previous study of *Magel2*-knockout male mice modeling the Prader-Willi and Schaaf-Yang neurodevelopmental syndromes associated to ASD also showed a decrease in AVP[+] fibers in LS[78]. *Magel2*-KO mice exhibit impaired social novelty preference[79], which can be rescued using AVP infusion in LS or optogenetic stimulation[78]. In our study, however, social novelty preference was not affected by chemogenetic silencing of BNST[AVP] cells (Supplementary Fig. S6e–i). Whether dysregulation of AVP inputs to LS is a common feature of ASD models and whether social deficits exhibited by other ASD models can be rescued by manipulating AVP signaling in LS remains to be explored.

Building on these findings, the discovery that AVPR1a promotes sociability while AVPR1b facilitates social aggression demonstrates how a single peptide release can facilitate separate behaviors via specific receptor activation. This segregation of action enabled us to selectivity rescue sociability in our ASD model without affecting social aggression. Previous studies in humans have demonstrated the potential for using AVP agonizts or AVPR1a antagonists to improve social deficits in children[80] or rescue social communications in adults[81–83] respectively, but without mechanism, these studies have generated limited interest. Our results open the way to novel AVP-based therapeutic approaches[84], aiming at rescuing sociability deficits in ASD patients without facilitating other undesirable behaviors such as social aggression.

Methods

Further information and requests for reagents may be directed to Felix Leroy (felxfel@aol.com).

Ethical approval

All the experimental procedures were in conformity with the directive 2010/63/EU of the European Parliament and of the Council, and the RD 53/2013 Spanish regulation on the protection of animals use for scientific purposes, approved by the government of the Autonomous Community of Valencia, under the supervision of the Consejo Superior de Investigaciones Científicas Committee for Animal use in Laboratory.

Animals

8- to 16-week-old male C57BL6/J (Jackson Laboratories, #000664), *Avp-Cre*^{+/-} mice (Jackson Laboratories, #023530) and *Shank3B*^{+/-} mice (Jackson Laboratories, #017688) were used as experimental subjects. For experiments with mutant mice, the same age wild-type (WT) littermates were used as the control group. Male Balb/cBy mice (Jackson Laboratories, #001026) were used as intruders during the resident intruder test, and C57BL6/J male mice (Jackson Laboratories, #000664) as stimulus mice during the social interaction tests.

Stereotaxic surgeries

Surgical procedure. Animals were anesthetized with isoflurane and placed in the stereotaxic apparatus. An intramuscular injection of Carprofen was used as an anti-inflammatory drug. Eyes were covered with ophthalmic gel (Viscotears 2 mg/g) to prevent corneal desiccation. The hair of the head was removed, and the tissue was sterilized. Following the opening of the head's tissue, a small craniotomy was performed above the target region, and a thin glass pipette was placed on the desired depth to deliver the viral content. Injections were performed using the nano-inject II (Drummond Scientific) with a rate of 23 nl every 11 s with a 10 s delay between each. The skin was then closed with surgical glue, and animals rested in a recovery chamber until restoration of normal locomotor activity.

Viral vectors. For anterograde tracing, 100 nL of AAV2/1 syn.-FLEX.GCaMP6f.WPRE.SV40 (Addgene, #100833-AAV1) was injected unilaterally in the posterior BNST of *Avp-Cre* mice (injection coordinates accordingly to the Allen Brain Atlas: AP: +0.02 mm, ML: ±0.75, DV: −4.75 from the cranium). These coordinates were used for all subsequent BNST injections.

- For retrograde tracing, 100 nl of the herpes simplex virus hEF1a.LSIL.GFP (Rachael Neve, Massachusetts General Hospital, #RN406) was injected into the LS of *Avp-Cre* mice (coordinates: AP: +0.24 mm, ML: ±0.50, DV: −3.30 from the cranium). These coordinates were used for all subsequent LS injections.
- For AVP[+] cell labeling in VGLUT1 experiments, AAV2/9EF1a.-DIO.hChR2 (E123T/T159C).eYFP8 (Addgene, #35509) was injected in the posterior BNST of *Avp-Cre* x *Shank3B*^{+/-} and WT controls mice.
- For chemogenetic experiment, 200 nl of AAV2/8 hSyn.-DIO.hM4D(Gi)-mCherry (Addgene, #44362-AAV8) was bilaterally

- injected in the posterior BNST of *Avp-Cre* mice and WT littermates.
- For fiber-photometry calcium recording, 100 nl of AAV2/1 syn.-FLEX.GCaMP6f.WPRE.SV40 (Addgene, #100833-AAV1) was bilaterally injected in the posterior BNST of *Avp-Cre* mice.
- For AVP biosensor recordings, 200 nl of AAV9-hSyn-AVP0.3 was unilaterally injected in LS of C57BL6/J.
- For optogenetic silencing experiments, 200 nl of AAV2/1 hSyn1-DIO-eOPN3-mScarlet-WPRE (Addgene, #125713-AAV1) was injected bilaterally in the posterior BNST of *Avp-Cre* and WT littermates.
- For the *Avp* knock-down experiment, 200 nl of AAV2/9 GFP.U6.anti-*Avp*-shRNA or AAV2/9 GFP.U6.scramble-shRNA (Vector Biolabs, #253437-shAAV) were injected bilaterally in the BNST of C57BL6/J mice as experimental or control condition respectively. All viruses expressed for a minimum of 2 weeks before the beginning of experiments, except for the shRNA-expressing AAVs, that expressed for 1 week only.

Fiber optic implants. Animals were anesthetized with isoflurane and placed in the stereotaxic apparatus. An intramuscular injection of Carprofen was used as an anti-inflammatory drug. The scalp was sterilized and completely removed. VetbondTM (3 M™ #7000002814) was applied on the peripheries of the cut to hold the tissue. Two screws were placed on the back of the cranium to provide a sturdy foundation for the implant. A craniotomy was performed above the target region, and an optical ferrule (200 μm core, black ceramic ferrule, Neurophotometrics) was lowered until the desired depth. Superglue was applied to hold the lens in position, and dental cement (GC FujiCEM 2) was applied to cover the exposed skull and to maintain the optical ferrule in place. For fiber-photometry calcium and vasopressin recordings, the optical ferrule implant was placed in LS at the following coordinates AP: + 0.24, ML: 0.5, DV: − 2.80 (from the cranium). For optogenetics silencing of BNST terminals, the optical ferrule implant was placed in LS at the following coordinates AP: + 0.24, ML: 0, DV: − 2.80 (from the cranium). Animals remained undisturbed for a week after the procedure.

Guide cannula implants. The mouse scalp was removed and scored before a hole was drilled (AP: + 0.24, ML: ± 0.00). A cannula guide extending 2.4 mm below the pedestal (Plastics One, #C315G 2-G11-SPC) was lowered slowly and kept in place using superglue. The skull was then covered with dental cement (GC FujiCEM 2), and dummy cannulas (Plastics One, #C315DC-SPC) were inserted into the guides. The mice were returned to their home cages and left to recover for at least 3 days. Mice were immobilized by the experimenter, and the dummy cannula was removed. A cannula (Plastics One, #C315I-SPC) projecting 1.7 mm from the tip of the cannula guide was mounted.

Histology and immunohistochemistry
Animals were anesthetized with isoflurane and intracardially perfused with 10 mL of saline. The brains were quickly extracted and incubated in 4% PFA overnight. The brains were washed for 1 h in PBS, and 50 μm slices of the regions of interest were sliced using a Leica VT1000S vibratome (Leica Biosystems).

Immunohistochemistry. The slices were permeabilized for 2 h in PBS with 0.5% Triton-X100 (T9284, Sigma-Aldrich) before being incubated overnight at 4 °C with primary antibodies diluted in PBS with 0.5% Triton-X in PBS. The slices were washed in PBS for 1 h, then incubated for 2 h or overnight at 4 °C with secondary antibodies from Thermo-Fisher Scientific at a concentration of 1:500 diluted in PBS with 0.1% Triton-X. Hoechst counterstain was applied (Hoechst 33342 at 1:1000 for 30 min in PBS at RT) prior to mounting the slice using fluoromount (Sigma-Aldrich).

c-fos labeling. For c-fos labeling, primary incubation was performed overnight at 4 °C with anti-c-fos antibody (1:1000, Abcam, #ab190289). Secondary incubation was performed with an anti-rabbit antibody conjugated to Alexa 488 (#A11039) at a concentration of 1:500 for 2 h at room temperature.

Anti-vasopressin labeling. For vasopressin labeling, primary incubation was performed overnight at 4 °C with anti-vasopressin antibody (1:1000, Merck, #PC234L). Secondary incubation was performed with an anti-rabbit antibody conjugated to Alexa 488 (#A11039) (1:500) overnight.

Anti-VGLUT1 labeling. For anti-VGLUT1 labeling, primary incubation was performed overnight at 4 °C with anti-VGLUT1 antibody (1:2000, Millipore, #ab5905). Secondary incubation was performed with an anti-guinea pig antibody conjugated to Alexa 594 (#A11076) (1:500) for 2 h at room temperature.

RFP labeling. For RFP labeling intensification of the signal, primary incubation was performed overnight at 4 °C with rabbit anti-RFP (1:500, Rockland Antibody, #600-401-379), and secondary incubation was performed with anti-rabbit antibody conjugated to Alexa 568 (#A11011) (1:500) for 2 h at room temperature.

GFP labeling. For intensification of the GFP labeling, primary incubation was performed overnight at 4 °C with and chicken anti-GFP (1:1000, Aves, #GFP-1020) antibodies. Secondary incubation was performed with anti-chicken antibody conjugated to 488 (#A11039) (1:500) overnight.

In situ hybridization
Animals were anesthetized using isoflurane and decapitated. The brains were quickly extracted and immersed in cooled 2-methylbutane for 6 s before being stored at 80 °C. 20 μm slices of the region of interest were prepared using a Leica cryostat (CM3050 S, Leica Biosystems) and mounted on Superfrost Plus microscope slides (12-550-15, FisherBrand). The slices were then processed following the RNAscope® Multiplex Fluorescent Detection Reagents v2 (CN:232110, ACD Bio) with the probes for *Avp* in C1 (#401391) and *Avpr1a* in C3 (#418061-C3). Protease IV was applied for 2 min, and TSA Vivid Dyes 520 was used to visualize *Avp* and 650 for *Avpr1a* DAPI was applied for 30 s prior to mounting using fluoromount.

Drugs
For hM4D activation, i.p. administration of clozapine-N-oxide dihydrochloride (CNO, Hello Bio, HB6149) dissolved in physiological saline (0.9% NaCl) at a dose of 3 mg kg−1 in a volume of 10 ml kg−1, was used 30 min before the behavioral experiments. I.p. injections of saline (0.9% NaCl) were used 30 min before the behavioral experiments as a control condition. All animals (control and ID) received i.p. CNO injections and saline injections. Saline experiments were performed with 3 days of interval for the sociability test and 1 week of interval for the resident-intruder test to prevent heightened aggression resulting from close repetitive exposure to an intruder in the home-cage.

For the guide cannula experiments on WT mice, C57BL/6 mice were infused in LS with 1 μl of saline, 1 μl of the AVPR1b antagonist SSR149415 at 2 μM, or 1 μl of the AVPR1a antagonist SR49059. For the guide cannula experiments on mutant mice, *Shank3B*+/- mice were infused in LS with 1 μl of saline, 1 μl of the AVPR1b agonist DDAVP at 100 μM solution, or 1 μl of AVP at 1 mM combined with together with the antagonist of AVPR1b, SSR149415 at 2 μM to selectively activate AVPR1a only. All drugs came from Tocris (Table 1). Drugs were infused at a rate of 0.2 μl per minute using a programmable syringe pump (Chemyix Inc.) mounted with a 2 μl syringe (Hamilton #88511). After infusion, animals were undisturbed for 5 min before the start of the

Table 1 | Reagents and resources information

REAGENT or RESOURCE	SOURCE	IDENTIFIER
Antibodies		
Anti-c-fos antibody produced in rabbit	Abcam	#ab190289 RRID:AB_2737414
Anti-GFP antibody produced in chicken	AVES Labs	#GFP-1020 RRID:AB_10000240
Anti-vasopressin antibody produced in a rabbit	Merck	#PC234L RRID:AB_565256
Anti-RFP antibody produced in a rabbit	Rockland Antibody	#600-401-379 RRID:AB_2209751
Anti-VGLUT1 antibody produced in a guinea pig	Merck	#ab5905 RRID:AB_2301751
Goat anti-rabbit IgG (H + L) secondary antibody, Alexa Fluor 488 conjugate	Thermo-Fisher Scientific	#A11039 RRID:AB_142924
Goat anti-rabbit IgG (H + L) secondary antibody, Alexa Fluor 568 conjugate	Thermo-Fisher Scientific	#A11011 RRID:AB_143157
Goat anti-guinea-pig IgG (H + L) secondary antibody, Alexa Fluor 594 conjugate	Thermo-Fisher Scientific	#A11076 RRID:AB 2534120
Goat Anti-chicken IgG (H + L) secondary antibody, Alexa Fluor 488 Conjugate	Thermo-Fisher Scientific	#A11039 RRID:AB_142924
In situ hybridization probes		
Avp in C1	ACD Bio	#401391
Avpr1a in C3	ACD Bio	#418061-C3
Chemicals, Peptides, and Recombinant Proteins		
CNO	Cayman Chemical	#16882
SR49059	Tocris	#2310
Desmopressin	Tocris	#3396
[Arg^8]-Vasopressin	Tocris	#2935
SSR149415	Tocris	#6195
Experimental Models: Organisms/Strains		
C57BL/6 J Mus musculus	Jackson Laboratories	RRID:IMSR_JAX:000664
Avp-Cre$^{+/-}$	Jackson Laboratories	RRID:IMSR_JAX:023530
Shank3B$^{+/-}$	Jackson Laboratories	RRID:IMSR_JAX:017688
Balb/cByJ	Jackson Laboratories	RRID:IMSR_JAX:001026
Recombinant DNA		
HSV hEF1a.LSIL.GFP (HT)	Massachusetts General Hospital	#RN406
AAV2/1 syn.FLEX.GCaMP6f.WPRE.SV40	Addgene	#100833-AAV1
AAV2/9EF1a.DIO.hChR2 (E123T/T159C).eYFP8	Addgene	#35509-AAV9
AAV2/8 hSyn.DIO.hM4D(Gi)-mCherry	Addgene	#44362-AAV8
AAV2/1 hSyn1-DIO-eOPN3-mScarlet-WPRE	Addgene	#125713-AAV1
AAV2/9 GFP.U6.anti-*Avp*-shRNA	Vector Biolabs	#253437-shAAV[50]
AAV2/9 GFP.U6.scramble-shRNA	Vector Biolabs	[50]
AAV9-hSyn-AVP0.3	Yulong Li	
Software		
PRISM 8	Graphpad	8.4.1 (455)
Microsoft Office Word	Microsoft	2019 16.56
Microsoft Office Excel	Microsoft	2019
Adobe Illustrator	Adobe	2023
Fiji	GPL v2	2.3.0/1.53 f
Python		3.10.2
MATLAB	Mathworks	2024b
Guppy	Lerner Lab[88]	1.1.4
SimpylCellCounter	https://github.com/aneeshbal/SimpylCellCounter[87]	2.0
Leica Application Suite X	Leica	v3.7.4
ANY-maze	Stoelting Co.	4.99
Bonsai	Open Ephys	2.8.2
Doric Neuroscience Studio	Doric	5.4.1.23

experiment. Drugs were randomized per animal during the sessions, and each session was performed with 3 days interval for the sociability test, and 1 week of interval for the resident-intruder test. For checking the guide cannula infusion localization in the brain, mini-Ruby (Invitrogen, D1868) was used. A total of 1 µl was infused at a rate of 0.2 µl per minute. 60 min after infusion, animals were perfused.

Behavioral tests

All animals were housed with littermates (maximum of 5 per cage) at a temperature of 24 °C with 12 h daily illumination and food and water ad libitum. The light cycle was not inverted, and experiments were conducted under dim light conditions.

Open arena test. Animals were placed in a white open arena (OA) (60 cm x 60 cm) and allowed to explore freely the space for 10 min. Automatic tracking software (Any-Maze 7, Stoelting) was used to quantify the time spent in the center and surroundings, as well as the total distance traveled by the animal.

Social interaction test. Animals were insolated in their home-cage, and 2 min calcium recording sessions were conducted in the empty home-cage. Subsequently, a stimulus mouse (Balb/cByJ) was introduced for another 2 min. Animals were allowed to freely explore, and the frequency and amplitude of the calcium signal was quantified for both conditions.

Sociability test. Wire cup cages were placed diagonally in opposite corners of the open arena. One of the cups was empty, and the other had a male, same-aged, unfamiliar mouse under it. Test subjects were allowed to freely explore the arena for 5 min. The same automatic tracking software described above was used to generate regions of interest around the cups and to provide an output of the total time spent interacting with both cups. A discrimination index was used to calculate the interaction time with both cups: (time with social cup − time with empty cup) / total interaction time.

Social novelty preference test. For the learning trial, mice were placed in the open arena containing two wire cups with one male same-age unfamiliar mouse under each cup. The cups were placed diagonally at opposite sides of the arena, and the test mouse could freely explore for 5 min. The test mouse was then single-housed in a chamber for 30 min. For the recall trial, one of the animals under the wire cup was replaced with a novel, unfamiliar mouse. The test mouse was then placed again in the open arena and could freely explore. The automated software for tracking was used for quantifying the interaction time with both animals under the cup. A discrimination index was used to calculate the interaction time with familiar and novel mouse for the recall condition: (time with novel − time with familiar) / total interaction time.

Resident-intruder test. Animals were single-housed in a cage with food and water ad libitum for a week prior to the testing day. During this week, animals were undisturbed, and the bedding of their cage was not changed in order to preserve odors that can favor the development of territoriality. Test mice were virgin and did not receive any sexual or aggressive experience during isolation. An intruder male mouse (Balb/cBy) was placed inside the cage, and the social interactions were recorded for 10 min. The software Any-Maze (Stoelting) was used for manual scoring of the social behaviors displayed. Similar to our previous study[40], the following social behaviors were quantified: **social exploration** (facial and ano-genital sniffing initiated by the resident mouse), **social dominance** (resident mouse rising onto its hindlimbs to scruff the intruder's head, as well as excessive allo-grooming, chasing or mounting) and **attack** (biting attack followed by fighting and tail rattling). We show example pictures (Fig. 1f), and

example videos can be found in our previous publication[40]. For the c-fos experiments, the same protocol was followed, but following completion of the test, animals were undisturbed for 60 min for the expression of the immediate-early gene and then perfused as previously described.

Development of the GRAB$_{AVP0.3}$ sensor

The development, optimization, and characterization strategy of the GRAB$_{AVP0.3}$ followed the methodology of our previously developed GRAB sensors[85]. The GRAB$_{AVP0.3}$ was developed based on human AVPR2 and optimized by mutagenesis screening of fluorescent protein, linker region, and GPCR. Then GRAB$_{AVP0.3}$ was cloned into a pAAV vector and packaged into an AAV virus for in vivo expression.

Fiber-photometry calcium recording data acquisition

Animals were habituated to the optical fiber patch cord for 1 day before the test. The optical fiber patch cord was placed on top of the mouse's implant, and the sociability test and resident-intruder test were performed as previously described while recording calcium activity from vasopressinergic BNST terminals in LS. Data acquisition was performed using the FP3002 system from Neurophotometrics controlled via Bonsai (Open-Ephys). LEDs delivering two excitation wavelengths (470 nm for detection of GCaMP6f signal and 415 nm for a calcium-independent control) intercalated at 40 Hz throughout recording sessions. Fluorescence emission was focused onto a CMOS sensor for detection, with a region of interest drawn around the end of the plug of the patch cord. A key press trigger was used in Bonsai to save the timestamps of precise social interactions aligned to the calcium signal (social exploration and biting).

Fiber-photometry vasopressin recording data acquisition

AVP biosensor data acquisition was conducted using a DORIC system (Basic FMC). Two LEDs (405 nm and 465 nm) were coupled to a fluorescence mini-cube (FMC) to deliver light into optical ferrules permanently implanted above the dLS. Light was delivered at a final intensity of 12 µW (465 nm) and 249.5 µW (405 nm) at the tip of the patch-cord. Emitted light between 420 and 450 nm (with 405 nm excitation) and 500 and 540 nm (with 465 nm excitation) were collected through the FMC on separate fiber-coupled Newport 2151 photo-receiver modules. The fluorescent signals were collected in AC-low mode and converted to voltage via the formula $V = PRG$, where V is the collected voltage, P is the optical input power in watts, R is the photodetector responsivity in amps/watts (0.2 – 0.4), and G is the trans-impedance gain of the amplifier. Raw signals and 405 nm excitation (isosbestic signal) were recorded using Doric Neuroscience Studio software.

Optogenetic silencing

Animals were habituated to the optical fiber patch cord for 1 day before the test. The optical fiber patch cord was placed on top of the mouse's implant, and the sociability test and resident-intruder test were performed as previously described. In the experimental condition of silencing, light stimulation was supplied using the Cobolt-Jive 561 nm, adjusted at 5 mW, and applied during all the testing time. In control conditions, mice were subjected to the test with the patch cord connected but with no light stimulation. The experimental and control conditions were randomized between batches of animals and performed with an interval of 3 days between the sociability test and 1 week between the resident-intruder test, to prevent heightened aggression resulting from close repetitive exposure to an intruder in the home-cage.

Data analysis

Quantification of the density of cell bodies. In situ hybridization was used to label AVP and Avpr1a mRNA in the BNST and LS of *Shank3B*^{+/-}

and WT littermates, as previously described. Equivalent-sized images of the anterior and posterior LS and BNST were acquired with an inverted confocal microscope (SPEII, Leica) with identical settings. The pictures were loaded in the software Fiji (Schneider et al., 2012) and subjected to manual quantification using the cell counting function.

Quantification of the density of axonal fibers. Immunohistochemistry for labeling vasopressin was performed accordingly to the descriptions above. Equivalent-sized images of the anterior and posterior LS of *Shank3b*^{+/-} and WT littermates were acquired with an epifluorescent microscope (Thunder, Leica). The settings for image acquisition was the same for all samples. The pictures were loaded in Fiji software and transformed in to an 8-bit image. A threshold was set to cover all the white pixels of the image, which corresponded to the GFP signal. A selection of the white pixels was then generated, and the area corresponding to the GFP labeling was measured. Data was plotted as the total area of GFP pixels labeled[86].

Quantification of density of VGLUT1 clusters. Immunohistochemistry for labeling VGLUT1 was performed accordingly to the descriptions above. For both *Shank3b*^{+/-} and WT controls, equivalent-sized images of the BNST were acquired (x63 magnification) with identical settings on a confocal microscope (SPEII, Leica). The images were then converted to 8-bit format using ImageJ. A threshold was uniformly applied to all images to enhance the detection and count the different VGLUT1 clusters present on the soma and fibers of AVP cells. Finally, the ROIs used to outline the AVP cells are associated with the number of clusters to generate the VGLUT1 synapse density for each quantified cell.

Quantification of c-fos + cells. The automated program SimpylCellCounter[87] was used for the quantification of c-fos^{+} cells. Equivalent-sized images from anterior and posterior BNST and LS of *Shank3B*^{+/-} and WT littermates were acquired with identical settings in the Thunder microscope (Leica) were loaded in the program. The software utilized binary thresholding and morphological functions from the open-source computer vision library OpenComputerVision (OpenCV) to identify and quantify the cells based on shape and size. The size was defined as 5, and the circularity threshold as 0.8. An output of the images with the quantified cells was generated, and the cells on the total area were plotted.

Fiber photometry and AVP biosensor data analysis. The Guppy software[88] was used for fiber photometry and AVP biosensor data analysis. The raw data and the behavioral timestamps were loaded, and the first seconds of recording were removed for artifact correction. A subtraction of the background fluorescence was calculated using a time-fitted running average of the 470 nm channel relative to the 415 nm control channel using a least squares polynomial fit of degree 1. The $\Delta F/F$ was calculated by subtracting the fitted control channel from the signal channel and dividing by the fitted control channel using the formula: (470−415 nm)/415 nm. A peak enveloping Fourier transform was applied to the $\Delta F/F$ signal across the entire trace to identify peaks in activity. The data was presented as the deviation of the $\Delta F/F$ from its mean (z-score) using the formula: ($\Delta F/F$ − mean of $\Delta F/F$/ Standard deviation of $\Delta F/F$). The z-score of each interaction of interest were analyzed during the sessions based on a time window of −3 to 3 s for the PSTH analysis. For the sociability test, the interaction with the object only (empty cup) was used as a control condition. For the resident-intruder test, the pre-biting or pre-social interaction transients were used as a control condition from −3 to −1 seconds. The area under the curve and the peak amplitude were plotted accordingly to these time windows.

Decoder analysis. Fiber photometry recordings of calcium or AVP biosensor signal were used to discriminate between non-social and social transients. In each session, we detected the transients and computed the peak amplitude and the area under the curve of each transient. To discriminate whether the recording came from a non-social or social condition, we trained linear support vector machine (SVM) decoders, using both peak amplitude and transient strength of all detected transients. We trained decoders by randomly selecting 70% data points as a training set and evaluated the decoder performance using the rest 30% as a testing set. To correct for class imbalance, as a standard procedure, we implemented a cost for misclassification that is inversely proportional to the number of samples in each class. This random sampling procedure was repeated 20 times to avoid sampling bias, and the results were averaged across repeats for each session. To generate a baseline distribution, we shuffled the labels (non-social vs social condition) of the data points and trained decoders as above. This shuffling procedure was repeated 1000 times. Decoder performance was evaluated as the area under the curve (AUC) of the receiver operating characteristic (ROC) curve. A statistical test (one-sided Wilcoxon signed-rank test) was performed to compare the AUC between the real data and the top 95% quantile of the shuffled distribution. For the biosensor data, we performed the decoder analysis to discriminate between social and non-social transients in WT and *Shank3B*^{+/-} mice, using the same procedure as described above.

Supervised annotation in DeepOF analysis. Videos of WT or *Shank3B*^{+/-} mice freely interacting in an open arena with a stimulus mouse were captured using a DMK 27BUR0135 (The IMAGING SOURCE) camera, positioned 130 cm above the arena for a top-down perspective. The recordings were acquired with Bonsai-RX software. Initially, the test mouse was allowed to explore the arena freely for 10 min. Following this, a stimulus mouse (BALB/c, males, 7−11 weeks old) was introduced into the arena, and a 2 min interaction period was recorded and saved for subsequent analysis. The interactions between the test and stimulus mice were analyzed using DeepOF software (version 0.7.2)[89,90]. To facilitate this, the body parts of both mice were tracked with DeepLabCut (version 2.2.3)[91] using a custom-trained model. DeepOF analysis was then conducted based on the calculated trajectories for each body part[89,90]. Finally, each frame was classified into specific behaviors using DeepOF's pre-trained network.

Statistics and reproducibility

Statistical analyses and figure plotting were performed using Prism version 9 (GraphPad). No statistical methods were used to pre-determine sample sizes, but sample size was selected based on previous experience and on estimation from related studies. Unless specified otherwise, bar graphs represent mean ± s.e.m. Sample sizes and statistical tests are reported in the figure legends. * indicates $p < 0.05$, ** indicates $p < 0.01$, *** indicates $p < 0.001$ and **** indicates $p < 0.0001$. When multiple observations were done in the same mouse, nested statistical tests were used to take into account the lower degree of freedom. Experiments using viral injections for anterograde and retrograde tracing were independently repeated a minimum of three times, producing similar outcomes. For experiments involving viral expression or optical ferrule implant, only animals exhibiting proper viral expression and accurate optical ferrule localization were included in the analysis.

Reporting summary

Further information on research design is available in the Nature Portfolio Reporting Summary linked to this article.

Data availability

The data generated in this study are provided in the Source Data file. Request for raw data files should be directed to Felix Leroy (felxfel@aol.com). Source data are provided in this paper.

Code availability

The code used to create the classifiers analysis of the fiber-photometry data is available at https://github.com/hanshuting/AVP_decoder_manuscript. Any additional information required to reanalyze the data reported in this paper is available from the lead contact upon request.

References

1. Harony, H. & Wagner, S. The contribution of oxytocin and vasopressin to mammalian social behavior: Potential role in Autism Spectrum Disorder. *Neurosignals* **18**, 82–97 (2010).
2. Lukas, M. & Neumann, I. D. Oxytocin and vasopressin in rodent behaviors related to social dysfunctions in autism spectrum disorders. *Behav. Brain Res.* **251**, 85–94 (2013).
3. Zhang, R., Zhang, H. F., Han, J. S. & Han, S. P. Genes related to oxytocin and arginine-vasopressin pathways: Associations with Autism Spectrum Disorders. *Neurosci. Bull.* **33**, 238–246 (2017).
4. Cataldo, I., Azhari, A. & Esposito, G. A review of oxytocin and arginine-vasopressin receptors and their modulation of Autism Spectrum Disorder. *Front. Mol. Neurosci.* **11**, https://doi.org/10.3389/fnmol.2018.00027 (2018).
5. Francis, S. M. et al. Variants in adjacent oxytocin/vasopressin gene region and associations with ASD diagnosis and other Autism autism-related endophenotypes. *Front. Neurosci.* **10**, https://doi.org/10.3389/fnins.2016.00195 (2016).
6. Dempster, E. L. et al. Further genetic evidence implicates the vasopressin system in childhood-onset mood disorders. *Eur. J. Neurosci.* **30**, 1615–1619 (2009).
7. Shou, X. J. et al. A volumetric and functional connectivity MRI study of brain arginine-vasopressin pathways in autistic children. *Neurosci. Bull.* **33**, 130–142 (2017).
8. Xu, X. J. et al. Mothers of autistic children: Lower plasma levels of oxytocin and arg-vasopressin and a higher level of testosterone. *PLoS ONE* **8**, https://doi.org/10.1371/journal.pone.0074849 (2013).
9. Zhang, H. F. et al. Plasma oxytocin and arginine-vasopressin levels in children with Autism Spectrum Disorder in China: associations with symptoms. *Neurosci. Bull.* **32**, 423–432 (2016).
10. Oztan, O. et al. Cerebrospinal fluid vasopressin and symptom severity in children with autism. *Ann. Neurol.* **84**, 611–615 (2018).
11. Oztan, O., Garner, J. P., Constantino, J. N. & Parker, K. J. Neonatal CSF vasopressin concentration predicts later medical record diagnoses of autism spectrum disorder. *Proc. Natl. Acad. Sci. USA* **117**, 10609–10613 (2020).
12. Carson, D. S. et al. Arginine Vasopressin Is a Blood-Based Biomarker of Social Functioning in Children with Autism. *PLoS ONE* **10**, e0132224 (2015).
13. Yirmiya, N. et al. Association between the arginine vasopressin 1a receptor (AVPR1a) gene and autism in a family-based study: mediation by socialization skills. *Mol. Psychiatry* **11**, 488–94 (2006).
14. Kim, S. J. et al. Transmission disequilibrium testing of arginine vasopressin receptor 1A (AVPR1A) polymorphisms in autism. *Mol. Psychiatry* **7**, 503–507 (2002).
15. Wassink, T. H. et al. Examination of AVPR1a as an autism susceptibility gene. *Mol. Psychiatry* **9**, 968–72 (2004).
16. Francis, S. M. et al. ASD and Genetic associations with receptors for oxytocin and vasopressin—AVPR1A, AVPR1B, and OXTR. *Front. Neurosci.* **10**, 516 (2016).
17. Dempster, E. L. et al. Evidence of an association between the vasopressin V1b receptor gene (AVPR1B) and childhood-onset mood disorders. *Arch. Gen. Psychiatry* **64**, 1189–1195 (2007).
18. Tansey, K. E. et al. Functionality of promoter microsatellites of arginine vasopressin receptor 1A (AVPR1A): implications for autism. *Mol. Autism* **2**, 3 (2011).
19. Yang, S. Y. et al. Family-based association study of microsatellites in the 5' flanking region of AVPR1A with autism spectrum disorder in the Korean population. *Psychiatry Res.* **178**, 199–201 (2010).
20. van den-Ouweland, A. M. W. et al. Mutations in the vasopressin type 2 receptor gene (AVPR2) associated with nephrogenic diabetes insipidus. *Nat. Genet.* **2**, 99–102 (1992).
21. Dantzer, R., Bluthe, R. M., Koob, G. F. & Le Moal, M. Modulation of social memory in male rats by neurohypophyseal peptides. *Psychopharmacology* **91**, 363–368 (1987).
22. Le Moal, M., Dantzer, R., Michaud, B. & Koob, G. F. Centrally injected arginine vasopressin (AVP) facilitates social memory in rats. *Neurosci. Lett.* **77**, 353–359 (1987).
23. Engelmann, M., Ludwig, M. & Landgraf, R. Simultaneous monitoring of intracerebral release and behavior: endogenous vasopressin improves social recognition. *J. Neuroendocrinol.* **6**, 391–395 (1994).
24. Dantzer, R., Koob, G. F., Bluthé, R. M. & Le Moal, M. Septal vasopressin modulates social memory in male rats. *Brain Res.* **457**, 143–147 (1988).
25. Bychowski, M. E., Mena, J. D. & Auger, C. J. Vasopressin infusion into the lateral septum of adult male rats rescues progesterone-induced impairment in social recognition. *Neuroscience* **246**, 52–58 (2013).
26. Bluthe, R.-M. & Dantzer, R. Social recognition does not involve vasopressinergic neurotransmission in female rats. *Brain Res.* **535**, 301–304 (1990).
27. van Wimersma Greidanus, T.jB. & Maigret, C. The role of limbic vasopressin and oxytocin in social recognition. *Brain Res.* **713**, 153–159 (1996).
28. Bielsky, I. F., Hu, S. B., Szegda, K. L., Westphal, H. & Young, L. J. Profound impairment in social recognition and reduction in anxiety-like behavior in vasopressin V1a receptor knockout mice. *Neuropsychopharmacology* **29**, 483–493 (2004).
29. Bielsky, I. F., Hu, S. B. & Young, L. J. Sexual dimorphism in the vasopressin system: lack of an altered behavioral phenotype in female V1a receptor knockout mice. *Behav. Brain Res.* **164**, 132–136 (2005).
30. Wersinger, S. R. et al. Vasopressin 1a receptor knockout mice have a subtle olfactory deficit but normal aggression. *Genes Brain Behav.* **6**, 540–551 (2007).
31. Caldwell, H., Wersinger, S. & Young, W. in *Advances in Vasopressin and Oxytocin; From Genes to Behaviour to Disease.* (Elsevier, 2008).
32. Sala, M. et al. Pharmacologic rescue of impaired cognitive flexibility, social deficits, increased aggression, and seizure susceptibility in oxytocin receptor null mice: A neurobehavioral model of Autism. *Biol. Psychiatry* **69**, 875–882 (2011).
33. Menon, R. et al. Neurobiology of the lateral septum: Regulation of social behavior. *Trends Neurosci.* **45**, 27–40 (2022).
34. Courchesne, E. Brainstem, cerebellar and limbic neuroanatomical abnormalities in autism. *Curr. Opin. Neurobiol.* **7**, 269–278 (1997).
35. Kotagiri, P., Chance, S. A., Szele, F. G. & Esiri, M. M. Subventricular zone cytoarchitecture changes in Autism. *Dev. Neurobiol.* **74**, 25–41 (2014).
36. Engelmann, M. & Landgraf, R. Microdialysis administration of vasopressin into the septum improves social recognition in Brattleboro rats. *Physiol. Behav.* **55**, 145–149 (1994).
37. De Vries, G. J., Buijs, R. M. & Van Leeuwen, F. W. Sex differences in vasopressin and other neurotransmitter systems in the brain. *Prog. Brain Res.* **61**, 185–203 (1984).
38. Rood, B. D. & De Vries, G. J. Vasopressin innervation of the mouse (Mus musculus) brain and spinal cord. *J. Comp. Neurol.* **519**, 2434–2474 (2011).
39. Rigney, N. et al. A vasopressin circuit that modulates mouse social investigation and anxiety-like behavior in a sex-specific manner.

Proc. Natl. Acad. Sci. USA **121**, https://doi.org/10.1073/pnas.2319641121 (2024).

40. Leroy, F. et al. A circuit from hippocampal CA2 to lateral septum disinhibits social aggression. *Nature* **564**, 213–218 (2018).

41. Peça, J. et al. Shank3 mutant mice display autistic-like behaviours and striatal dysfunction. *Nature* **472**, 437–442 (2011).

42. Sgritta, M. et al. Mechanisms underlying microbial-mediated changes in social behavior in mouse models of Autism Spectrum Disorder. *Neuron* **101**, 246–259 (2019).

43. Koolhaas, J. M. et al. The Resident-Intruder Paradigm: A standardized test for aggression, violence and social stress. *J. Vis. Exp.* **77**, e4367 (2013).

44. Velez, L., Sokoloff, G., Miczek, K. A., Palmer, A. A. & Dulawa, S. C. Differences in aggressive behavior and DNA copy number variants between BALB/cJ and BALB/cByJ substrains. *Behav. Genet.* **40**, 201 (2010).

45. Sheng, M. & Kim, E. The Shank family of scaffold proteins. *J. Cell Sci.* **113**, 1851–1856 (2000).

46. Wang, M. et al. Decrease of GSK-3β activity in the anterior cingulate cortex of Shank3b−/− mice contributes to synaptic and social deficiency. *Front. Cell Neurosci.* **13**, https://doi.org/10.3389/fncel.2019.00447 (2019).

47. Bozdagi, O. et al. Haploinsufficiency of the autism-associated Shank3 gene leads to deficits in synaptic function, social interaction, and social communication. *Mol. Autism* **1**, (2010).

48. Leroy, F. et al. Enkephalin release from VIP interneurons in the hippocampal CA2/3a region mediates heterosynaptic plasticity and social memory. *Mol. Psychiatry* **27**, 2879 (2022).

49. Mahn, M. et al. Efficient optogenetic silencing of neurotransmitter release with a mosquito rhodopsin. *Neuron* **109**, 1621–1635 (2021).

50. Rigney, N., Zbib, A., de Vries, G. J. & Petrulis, A. Knockdown of sexually differentiated vasopressin expression in the bed nucleus of the stria terminalis reduces social and sexual behaviour in male, but not female, mice. *J. Neuroendocrinol.* **34**, https://doi.org/10.1111/jne.13083 (2022).

51. Zai, C. C. et al. Possible genetic association between vasopressin receptor 1B and child aggression. *Psychiatry Res.* **200**, 784–788 (2012).

52. Bielsky, I. F., Hu, S.-B., Ren, X., Terwilliger, E. F. & Young, L. J. The V1a vasopressin receptor is necessary and sufficient for normal social recognition: A gene replacement study. *Neuron* **47**, 503–513 (2005).

53. Besnard, A. & Leroy, F. Top-down regulation of motivated behaviors via lateral septum sub-circuits. *Mol Psychiatry* **8**, 3119–3128 (2022).

54. Trainor, B. C., Greiwe, K. M. & Nelson, R. J. Individual differences in estrogen receptor alpha in select brain nuclei are associated with individual differences in aggression. *Horm. Behav.* **50**, 338–345 (2006).

55. Beiderbeck, D. I., Neumann, I. D. & Veenema, A. H. Differences in intermale aggression are accompanied by opposite vasopressin release patterns within the septum in rats bred for low and high anxiety. *Eur. J. Neurosci.* **26**, 3597–3605 (2007).

56. Veenema, A. H., Beiderbeck, D. I., Lukas, M. & Neumann, I. D. Distinct correlations of vasopressin release within the lateral septum and the bed nucleus of the stria terminalis with the display of intermale aggression. *Horm. Behav.* **58**, 273–81 (2010).

57. Oliveira, V. E. de M. in *Handbook of Anger, Aggression, and Violence*. (2023).

58. Dai, B. et al. Experience-dependent dopamine modulation of male aggression. *Nature* **639**, 430–437 (2025).

59. Takahashi, A. & Miczek, K. A. Neurogenetics of aggressive behavior: Studies in rodents. *Curr. Top. Behav. Neurosci.* **17**, 3–44 (2013).

60. Trainor, B. C. & Nelson, R. J. in *Handbook of Neuroendocrinology*. (2012).

61. Witchey, S. K., Stevenson, E. L. & Caldwell, H. K. Genotypic differences in intruder-evoked immediate early gene activation in male, but not female, vasopressin 1b receptor knockout mice. *BMC Neurosci.* **17**, https://doi.org/10.1186/s12868-016-0310-7 (2016).

62. Young, W. S., Li, J., Wersinger, S. R. & Palkovits, M. The vasopressin 1b receptor is prominent in the hippocampal area CA2 where it is unaffected by restraint stress or adrenalectomy. *Neuroscience* **143**, 1031–1039 (2006).

63. Sun, Y., Zweifel, L. S., Holmes, T. C. & Xu, X. Whole-brain input mapping of the lateral versus medial anterodorsal bed nucleus of the stria terminalis in the mouse. *Neurobiol. Stress* **23**, https://doi.org/10.1016/j.ynstr.2023.100527 (2023).

64. Wersinger, S. R., Ginns, E. I., O'Carroll, A.-M., Lolait, S. J. & Young, W. S. III Vasopressin V1b receptor knockout reduces aggressive behavior in male mice. *Mol. Psychiatry* **7**, 975–984 (2002).

65. Luo, A. H., Tahsili-Fahadan, P., Wise, R. A., Lupica, C. R. & Aston-Jones, G. Linking Context with reward: A functional circuit from hippocampal CA3 to ventral tegmental area. *Science* **333**, 353–357 (2011).

66. Wang, Z., Bullock, N. A. & De Vries, G. J. Sexual differentiation of vasopressin projections of the bed nucleus of the stria terminals and medial amygdaloid nucleus in rats. *Endocrinology* **132**, 2299–2306 (1993).

67. Rigney, N., Whylings, J., Mieda, M., De Vries, G. J. & Petrulis, A. Sexually dimorphic vasopressin cells modulate social investigation and communication in sex-specific ways. *eNeuro* **6**, https://doi.org/10.1523/eneuro.0415-18.2019 (2019).

68. Bluthe, R. M., Schoenen, J. & Dantzer, R. Androgen-dependent vasopressinergic neurons are involved in social recognition in rats. *Brain Res.* **519**, 150–157 (1990).

69. Auger, C. J. & Vanzo, R. J. Progesterone treatment of adult male rats suppresses arginine vasopressin expression in the bed nucleus of the stria terminalis and the centromedial amygdala. *J. Neuroendocrinol.* **18**, 187–194 (2006).

70. Bychowski, M. E. & Auger, C. J. Progesterone impairs social recognition in male rats. *Horm. Behav.* **61**, 598–604 (2012).

71. Appenrodt, E., Juszczak, M. & Schwarzberg, H. Septal vasopressin induced preservation of social recognition in rats was abolished by pinealectomy. *Behav. Brain Res.* **134**, 67–73 (2002).

72. Dluzen, D. E., Muraoka, S. & Landgraf, R. Olfactory bulb norepinephrine depletion abolishes vasopressin and oxytocin preservation of social recognition responses in rats. *Neurosci. Lett.* **254**, 161–164 (1998).

73. Oliveira, V. E. de M. et al. Oxytocin and vasopressin within the ventral and dorsal lateral septum modulate aggression in female rats. *Nat. Commun.* **12**, 2900 (2021).

74. Veenema, A. H., Bredewold, R. & De Vries, G. J. Sex-specific modulation of juvenile social play by vasopressin. *Psychoneuroendocrinology* **38**, 2554–2561 (2013).

75. Bredewold, R., Smith, C. J. W., Dumais, K. M. & Veenema, A. H. Sex-specific modulation of juvenile social play behavior by vasopressin and oxytocin depends on social context. *Front. Behav. Neurosci.* **8**, https://doi.org/10.3389/fnbeh.2014.00216 (2014).

76. Nephew, B. C. & Bridges, R. S. Arginine vasopressin V1a receptor antagonist impairs maternal memory in rats. *Physiol. Behav.* **95**, 182–186 (2008).

77. Rigney, N., de Vries, G. J. & Petrulis, A. Modulation of social behavior by distinct vasopressin sources. *Front. Endocrinol.* **14**, https://doi.org/10.3389/fendo.2023.1127792 (2023).

78. Borie, A. M. et al. Correction of vasopressin deficit in the lateral septum ameliorates social deficits of the mouse autism model. *J. Clin. Invest.* **131**, https://doi.org/10.1172/jci144450 (2021).

79. Fountain, M. D., Tao, H., Chen, C. A., Yin, J. & Schaaf, C. P. Magel2 knockout mice manifest altered social phenotypes and a deficit in preference for social novelty. *Genes Brain Behav.* **16**, 592–600 (2017).

80. Parker, K. J. et al. A randomized placebo-controlled pilot trial shows that intranasal vasopressin improves social deficits in children with autism. *Sci. Transl. Med* **11**, https://doi.org/10.1126/scitranslmed.aau7356 (2019).

81. Hollander, E. et al. Balovaptan vs placebo for social communication in childhood Autism spectrum disorder: A randomized clinical trial. *JAMA Psychiatry* **79**, 760–769 (2022).

82. Schnider, P. et al. Discovery of balovaptan, a vasopressin 1a receptor antagonist for the treatment of Autism Spectrum Disorder. *J. Med. Chem.* **63**, 1511–1525 (2020).

83. Bolognani, F. et al. A phase 2 clinical trial of a vasopressin V1a receptor antagonist shows improved adaptive behaviors in men with autism spectrum disorder. *Sci. Transl. Med.* **11**, https://doi.org/10.1126/scitranslmed.aat7838 (2019).

84. László, K. et al. Vasopressin as possible treatment option in Autism Spectrum Disorder. *Biomedicines* **11**, https://doi.org/10.3390/biomedicines11102603 (2023).

85. Wang, H. et al. A tool kit of highly selective and sensitive genetically encoded neuropeptide sensors. *Science* **382**, https://doi.org/10.1126/science.abq8173 (2023).

86. Montanari, R. et al. Callosal inputs generate side-invariant receptive fields in the barrel cortex. *Sci. Adv.* **9**, https://doi.org/10.1126/sciadv.adi3728 (2023).

87. Bal, A., Maureira, F. & Arguello, A. A. SimpylCellCounter: an automated solution for quantifying cells in brain tissue. *Sci. Rep.* **10**, 12570 (2020).

88. Sherathiya, V. N., Schaid, M. D., Seiler, J. L., Lopez, G. C. & Lerner, T. N. GuPPy, a Python toolbox for the analysis of fiber photometry data. *Sci. Rep.* **11**, 1–9 (2021).

89. Miranda, L., Bordes, J., Pütz, B., Schmidt, M. V. & Müller-Myhsok, B. DeepOF: a Python package for supervised and unsupervised pattern recognition in mice motion tracking data. *J. Open Source Softw.* **8**, 5394 (2023).

90. Bordes, J. et al. Automatically annotated motion tracking identifies a distinct social behavioral profile following chronic social defeat stress. *Nat. Commun.* **14**, 4319 (2023).

91. Mathis, A. et al. DeepLabCut: markerless pose estimation of user-defined body parts with deep learning. *Nat. Neurosci.* **21**, 1281–1289 (2018).

Acknowledgements

Author contributions

Conceptualization: M.H.B-G. and F.L. Investigation: M.H.B-G., G.B., L.G., A.R.P. Y.N., and S.H. Writing – original draft: M.H.B-G. Writing – review & editing: M.H.B-G. and F.L. Visualization: M.H.B-G. Supervision: F.L. Funding acquisition: M.H.B-G., Y.L., F.L.

Competing interests

The authors declare no competing interests.

Additional information